Poly(ethylene glycol)-conjugated Phospholipids in Aqueous Micellar Solutions: Hydration, Static Structure, and Interparticle Interactions

Takaaki Sato,† Hiromi Sakai,† Keitaro Sou,† Richard Buchner,‡ and Eishun Tsuchida†,*

Advanced Research Institute for Science and Engineering, Waseda University, Okubo 3-4-1, Shinjuku-ku, Tokyo 169-8555, Japan, and Institut für Physikalische und Theoretische Chemie, Universität Regensburg, D-93040 Regensburg, Germany

Received: October 25, 2006; In Final Form: November 30, 2006

By means of dielectric relaxation spectroscopy (DRS) and small-angle X-ray scattering (SAXS), we have investigated hydration behavior, solvent dynamics, and static structures of aqueous solutions of poly(ethylene glycol)-conjugated distearoyl phosphatidylethanolamine (DSPE-PEG) (molecular weight of PEG: M_{PEG} = 2000, 5000, and 12 000 Da). A quantitative analysis of the bulk-water relaxation amplitude revealed the effective hydration number of a DSPE-PEG molecule per ethylene oxide monomer unit to be ~5.0−5.5, virtually independent of M_{PEG}. The overall hydration number of a DSPE-PEG molecule is ca. 20% higher than that of the corresponding normal PEG (without DSPE). This is attributed to both hydration of a charged head group of phosphoric acid in DSPE and a packing effect of PEG chains into micellar structures. The pair-distance distribution functions, $p(r)$, extracted from the GIFT analysis of SAXS intensities show that the DSPE-PEGs form spherical-like micelles in water having the maximum diameter of ~16, 22, and 31 nm, respectively, for M_{PEG} = 2000, 5000, and 12 000 Da and nearly identical aggregation numbers of 72 (±10%). The DSPE-PEG micelles behave as charged colloids whose interparticle interaction potential can be approximated by the screened Coulomb potential model. The extracted pair correlation function $g(r)$ demonstrates that both electrostatic repulsion induced by the charged head group and excluded volume effects of the fully hydrated PEG layer contribute to repulsive interactions among the PEG-lipid micelles. This should be a key factor for the function of PEG lipids as a stabilizer of liposomes.

1. Introduction

The hydrophobic driving forces, the solvent−water mediated segregating tendency of hydrophobic molecules or units, play a vital role in various self-assembly phenomena, ranging from the formation of molecular clusters to micelles and vesicular structures.[1] One example is the phospholipid vesicle or liposome that has extensively been studied as a drug delivery system since the formation of a vesicular structure was discovered in the suspension of egg-yolk phosphatidylcholine.[2] Some liposomes are now approved for clinical use as antifungal or anticancer therapies.[3] Poly(ethylene glycol) (PEG)-conjugated phospholipids (PEG-phospholipids) have widely been recognized as efficient stabilizers of phospholipid vesicles or liposomes.[4−6]

They are also effective for the vesicles used to encapsulate concentrated hemoglobin (Hb-vesicles, HbV) that have been developed as an artificial oxygen carrier.[7] Sakai, Sou, Tsuchida, and co-workers have confirmed that the surface modification of liposomes by an incorporation of PEG-phospholipids on the surface of HbV is effective for the stabilization of the vesicles. Long-term preservation of HbV dispersions is improved by suppressing the tendency for conventional liposomes to aggregate with subsequent sedimentation.[8,9] The stabilization has also been found to be useful for biocompatibility, microcirculatory blood flow, and prolonged circulation in the blood stream.[10−12] So far, the underlying mechanism of such stabilization has mainly been explained in terms of the steric hindrance or the excluded volume effect of the extended and hydrated PEG chains on the surface,[13] and the fundamental structural and physicochemical properties of PEG-phospholipids in micellar systems were studied by several authors.[14,15] However, specific knowledge of the hydration of PEG chains in PEG-phospholipid micelles and of the geometric profiles of the micelles, that would be of cardinal importance to elucidate the stabilizing mechanism provided by PEG-phospholipids, is still rare.

Here, we investigated static structures and molecular to cooperative dynamics of aqueous solutions of a series of PEG-conjugated phospholipids, aiming at elucidating key properties that contribute to the stabilization of liposomes. The unique combination of dielectric relaxation spectroscopy (DRS) and small-angle X-ray scattering (SAXS) provides an eminent tool to investigate diverse aspects of aqueous PEG-phospholipid solutions, such as hydration behavior, solvent dynamics, static structures, and intermicellar interaction potentials.

Owing to its eminent sensitivity to all kinds of polarization fluctuations occurring in the nano- to picosecond time scales, DRS[16−26] has proven to be a powerful method for scrutinizing the wide-ranged multifaceted dynamical properties of liquids, involving collective dynamics of solvent,[17−19] hydration,[20−22] micellar specific processes,[23,24] and so on. By an elaborate least-squares fitting procedure of the complex dielectric spectrum, the relaxation times and amplitudes for polarization fluctuations of different physical origins can separately be extracted for further quantitative analysis. DRS is generally regarded as a "mature" technique, but it has only recently reached sufficient accuracy and resolution that enables successful application to

* To whom correspondence should be addressed. E-mail: eishun@waseda.jp. Phone: +81-3-5286-3120. Fax: +81-3-3205-4740.
† Advanced Research Institute for Science and Engineering.
‡ Institut für Physikalische und Theoretische Chemie.

10.1021/jp067011k CCC: $37.00
Published on Web 01/18/2007

ionic and non-ionic micellar solutions typically showing multistep relaxation behavior.[20-24]

On the one hand, SAXS[21,27-37] is a widely applied technique to investigate the structure and interaction potential of colloids, e.g., micelles, vesicles, and proteins, whose length scale is typically within the range of 1~100 nm. The generalized indirect Fourier transformation (GIFT) technique[32-36] developed by Glatter and co-workers in the past decade as an extension of the well-established indirect Fourier transformation (IFT) technique[29] has renovated situations in small-angle scattering (SAS) data analysis. GIFT allows us to access virtually model-free real space structural information on the nanoassemble systems even for the strongly interacting dense systems.

2. Experimental Section

2.1. Materials. Poly(ethylene glycol)-conjugated phospholipids, 1,2-distearoyl-*sn*-glycero-3-phosphatidylethanolamine-*N*-[monomethoxy-poly(ethylene glycol)], hereafter abbreviated as DSPE-PEG, having PEG of molar mass of 2000, 5000, and 12 000 Da and poly(ethylene glycol)s (PEGs) with molecular masses of 2000, 5000, and 12 000 Da were purchased from NOF Co. (Tokyo, Japan).

2.2. Sample Preparation. Solutions were prepared by weight from solid samples of DSPE-PEG and PEG (M_{PEG} = 2000, 5000, and 12 000 Da) by adding Millipore (Milli-Q) water. According to the procedure of Johnsson et al., DSPE-PEG solutions were incubated at ~60 °C for about 3 h. These freshly prepared solutions were kept for a half day at ambient temperature for equilibration and were immediately used for dielectric relaxation spectroscopy (DRS) and small-angle X-ray scattering (SAXS) experiments.

2.3. Dielectric Relaxation Spectroscopy (DRS). To obtain specific information about hydration of hydrophilic groups and states of water in aqueous DSPE-PEG systems from the view point of molecular dynamics, we have determined the complex dielectric spectra, $\epsilon^*(\nu) = \epsilon'(\nu) - i\epsilon''(\nu)$, of these aqueous solutions at 25 °C in the frequency range $0.03 \le \nu/\mathrm{GHz} \le 20$ by the use of time domain reflectometry (TDR)[18,19] based on the Hewlett-Packard instruments HP54121A and HP54120B. All time-domain measurements and conversion of the time-domain reflected plus waveforms to the frequency-domain spectrum were made according to the previously reported procedure of Sato and Buchner.[18] For selected systems, the frequency range was expended to the millimeter-wave region by the use of A-band and E-band waveguide interferometry,[26] covering $27 \le \nu/\mathrm{GHz} \le 89$. For the quantitative description of the experimental $\epsilon^*(\nu)$ spectra, we have tested various conceivable relaxation models based on a superposition of n Havriliak-Negami (HN) equations, or its variants, using a nonlinear least-squares fitting procedure

$$\epsilon^*(\nu) = \epsilon_\infty + \sum_{j=1}^{n} \frac{\Delta\epsilon_j}{[1 + (i2\pi\nu\tau_j)^{\beta_j}]^{\alpha_j}} \quad (1)$$

In these models, the jth dispersion step (j = 1, 2, ..., n) is defined by its relaxation time, τ_j ($\tau_j > \tau_{j+1}$), and amplitude, $\Delta\epsilon_j$, where n is the number of the separable dispersion steps. ϵ_∞ is the infinite frequency permittivity, and α_j and β_j are the shape parameters representing asymmetric and symmetric shapes of a spectrum, respectively.

2.4. Small-Angle X-ray Scattering (SAXS). All SAXS experiments were performed using a SAXSess camera (Anton-Paar, Graz, Austria). A PW3830 X-ray generator with a long fine focus sealed glass X-ray tube (PANalytical) was operated at 40 kV and 50 mA. A focusing multilayer optics and a block collimator provide an intense monochromatic primary beam (Cu Kα radiation, λ = 0.154 nm) with negligible background. A semi-transparent beam stop enables measurement of the attenuated primary beam at q = 0. The samples were filled into vacuum-tight thin quartz capillaries and set in a TCS 120 temperature-controlled sample holder unit (Anton Paar). The 2D scattered intensity distribution recorded by an imaging-plate (IP) detector was read out by a Cyclone storage phosphor system (Perkin-Elmer, USA). The 2D data were integrated into the 1D scattering function $I(q)$ as a function of the magnitude of the scattering vector

$$q = \frac{4\pi}{\lambda}\sin(\theta/2) \quad (2)$$

where θ is the total scattering angle.

All $I(q)$ data were normalized so as to have the uniform primary intensity at q = 0 for transmission calibration. The background scattering contributions from capillary and solvent were corrected. The absolute intensity calibration was made by using water intensity as a secondary standard.

2.5. Theoretical Basis of SAXS Data Analysis. The total scattered intensity, $I(q)$, from one-component globular particle systems can generally be formulated as

$$I(q) = n\,P(q)\,S(q) \quad (3)$$

where n is the particle density, $P(q)$ is the averaged form factor, and $S(q)$ is the static structure factor. SAXS observes the structure of nanoparticles via the convolution square (or the spatial autocorrelation function) of the electron density fluctuations

$$\gamma(r) \equiv \Delta\tilde{\rho}^2(r) = \langle\Delta\tilde{\rho}^2(r)\rangle = \langle\int_{-\infty}^{\infty}\Delta\rho(r_1)\Delta\rho(r_1 - r)\,dr_1\rangle \quad (4)$$

where $\Delta\rho(r)$ is the electron density fluctuation at the position r, and r is the distance between two scattering centers chosen inside the particle. The so-called pair-distance distribution function (PDDF), defined as $p(r) = \gamma(r)\,r^2$, is an essential real-space function that contains information on the geometry (size and shape) as well as the internal density fluctuation of the particle. $P(q)$ is the reciprocal-space coordinate associated with $p(r)$, and they are connected via the Fourier transformation

$$P(q) = 4\pi\int_0^\infty p(r)\frac{\sin qr}{qr}\,dr \quad (5)$$

The static structure factor $S(q)$ embodies a (time-averaged) length-scale dependent (particle) density fluctuation and therefore offers information about interparticle potentials of colloidal systems. $S(q)$ is given by the Fourier transformation of the total correlation function, $h(r) = g(r) - 1$, as

$$S(q) = 1 + 4\pi n\int_0^\infty [g(r) - 1]r^2\frac{\sin qr}{qr}dr \quad (6)$$

where $g(r)$ is the pair-correlation function. The SAXS data for aqueous DSPE-PEG solutions were analyzed by the generalized indirect Fourier transformation (GIFT) technique.

3. Results and Discussions

3.1. Dielectric Relaxation Behavior of Aqueous DSPE-PEG Solutions. In Figure 1, we present representative complex

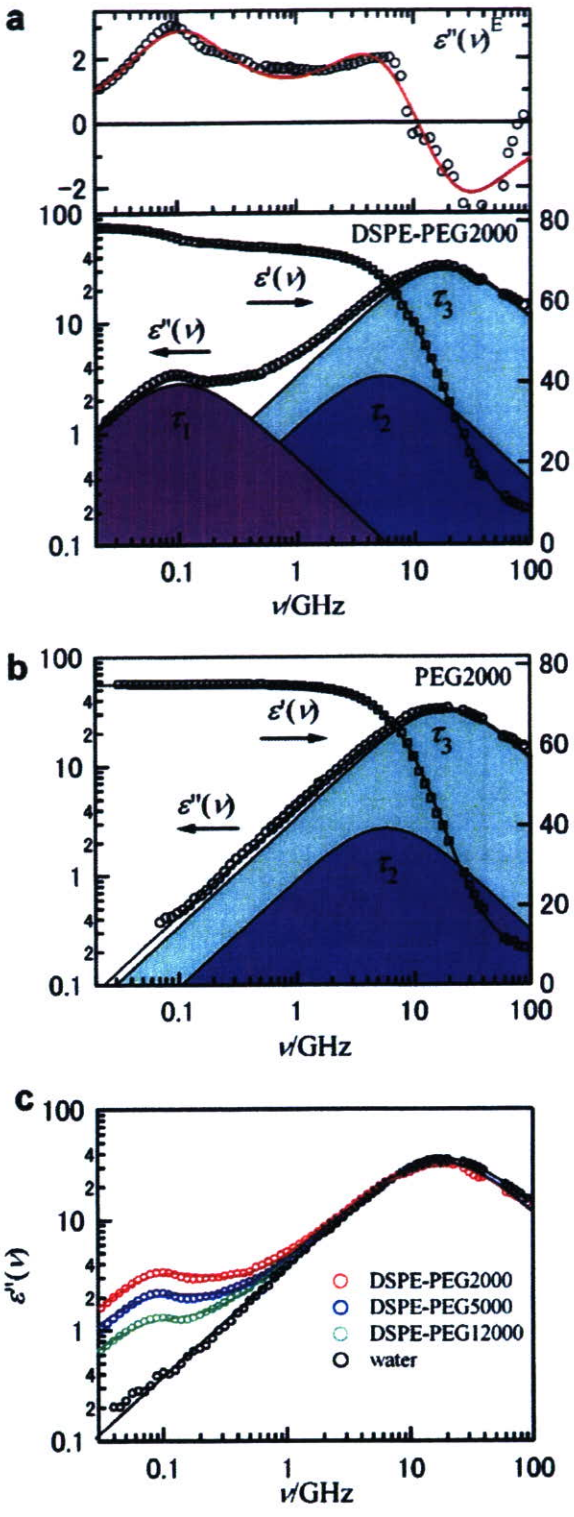

Figure 1. The complex dielectric spectra of aqueous DSPE-PEG and PEG solutions in $0.03 \leq \nu/\mathrm{GHz} \leq 89$ at 25 ± 0.03 °C. The spectrum of aqueous DSPE-PEG at polymer concentration $c = 7.1$ g dL^{-1} (a) and that of PEG at $c = 5.1$ g dL^{-1} (b), corresponding to $W_{\mathrm{PEG}} = 0.05$. In the upper panel of (a), the excess loss spectrum defined as $\epsilon''(\nu)^{\mathrm{E}} = \epsilon''(\nu) - \epsilon_{\mathrm{w}}''(\nu)$ is also shown, where $\epsilon_{\mathrm{w}}''(\nu)$ is an ideal bulk-water loss spectrum scaled according to analytical water concentration $c_{\mathrm{w}}(c)$. The comparison among DSPE-PEGs with different molecular masses of PEG, $M_{\mathrm{PEG}} = 2000$, 5000, and 12 000, at fixed $W_{\mathrm{PEG}} = 0.05$ (c), where the water spectrum from ref 17 is also shown for comparison.

dielectric spectra of aqueous DSPE-PEG and PEG solutions at 25 °C. An addition of either DSPE-PEG or PEG to water induces a pronounced broadening of the $\epsilon^*(\nu)$ spectrum on the lower frequency side of the loss peak frequency; the loss peak frequency centered at ~19 GHz remains virtually unchanged. The interferometry data covering up to 89 GHz confirm that there is no significant broadening of the high-frequency part of the spectrum. Thus, the low-frequency broadening is not likely due to a Cole−Cole-like relaxation-time distribution of the bulk water process but is validly attributed to the emergence of a new slow process. This also confirms the validity of the interpretation given in a recent dielectric study of Shikata et al.[22] on aqueous poly(ethylene oxide)s, where the frequency coverage was limited up to 20 GHz.

The observation of an almost constant loss peak frequency is fairly different from that of the situation for, e.g., alcohol/water mixtures,[18,19] where the loss peak frequency is continuously and rapidly sifted to lower frequencies with increasing solute concentration. The excess loss spectrum shown in the upper panel of Figure 1a indicates that, without imposing any relaxation model, two additional relaxation processes emerge upon addition of DSPE-PEG that are centered at ~100 MHz and ~5 GHz. Simultaneously, a negative excess polarization fluctuation appears for bulk-water relaxation without exhibiting a significant shift of the loss peak frequency. As for the results of the fitting procedure, we confirmed that a superposition of three Debye ($j = 3$) relaxation processes described as

$$\epsilon^*(\nu) = \epsilon_\infty + \sum_{j=1}^{3} \frac{\Delta\epsilon_j}{1 + 2i\pi\nu\tau_j} \tag{7}$$

gives the best description to the spectra for all the aqueous DSPE-PEGs (MPEG = 2000, 5000, and 12 000) and a consistent set of fitting parameters, whereas the corresponding normal PEG (without DSPE) solutions show only two dispersion steps, lacking the well-pronounced 100 MHz dispersion for DSPE-PEG solutions.

Figures 2 and 3 show the relaxation times τ_j and amplitudes $\Delta\epsilon_j$ of aqueous DSPE-PEG and PEG solutions, respectively. The relaxation times of the dominating high-frequency process, τ_3, of both DSPE-PEG and PEG solutions, are practically identical to that of the main dispersion of pure water, $\tau_{\mathrm{D}} = 8.3$ ps, and almost independent of polymer concentration, c, and molecular weight, M. As demonstrated by Figure 3, the amplitude, $\Delta\epsilon_3$, smoothly decreases from that for pure water with increasing c. Thus, the assignment of the τ_3-process is straightforward; this can clearly be attributed to the cooperative rearrangement of the hydrogen-bond network of bulk-like water. Note that, as already indicated by the negative excess loss spectrum at high-frequencies and demonstrated by Figure 3a, $\Delta\epsilon_3$ always exhibits smaller values than expected from analytical water concentration.

Neither the intermediate relaxation nor the lowest-frequency one can be attributed to the rotational diffusion of a whole DSPE-PEG micelle because τ_1 and τ_2 are too small if referring to the prediction of the Stokes−Einstein−Debye (SED) equation for the micellar radius determined from SAXS experiments (cf. Section 3.3). The τ_2-process centered at 5−6 GHz cannot necessarily be attributed to a micelle-specific process because the features are common to DSPE-PEG and normal PEG solutions. Judging from the time scale of τ_2, which is greater than that of bulk-water relaxation by a factor of 3 to 4, and from the behavior of $\Delta\epsilon_2$, which almost proportionally increases with c, the intermediate τ_2-relaxation is related to cooperative

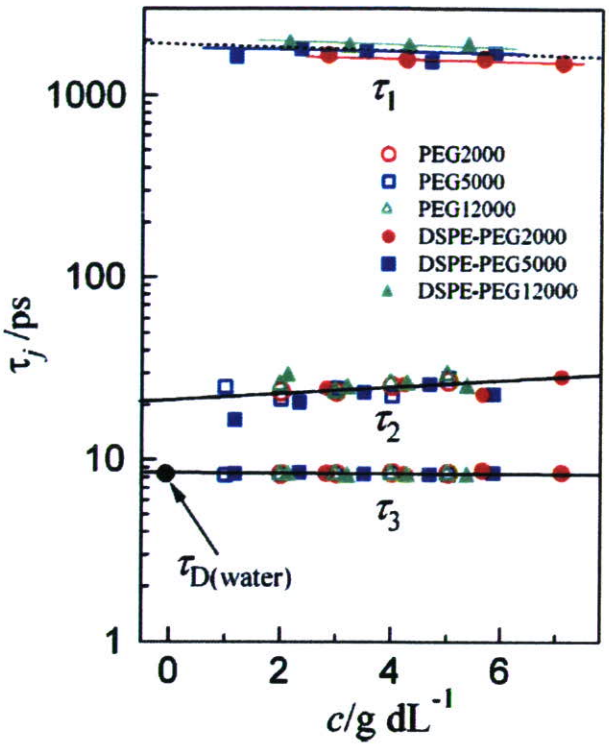

Figure 2. Dielectric relaxation times of aqueous solutions of DSPE-PEG and PEG for M_{PEG} = 2000, 5000, and 12 000 at 25 °C as a function of polymer concentration, c.

molecular motions in hydrated PEG layers. This is in line with the interpretation of dielectric spectra of the water/poly(oxyethylene) alkylether system given by Schrödle et al.[20] The process must be highly cooperative in the densely packed hydrated PEG layer because the conformational change of the poly(oxyethylene) chains and displacement of water molecules are required to occur simultaneously, leading to the sufficiently slower dielectric relaxation time compared to that of bulk water.

The low-frequency relaxation process characterized by $\tau_1 \sim 2$ ns (loss peak frequency ~ 0.1 GHz) exists only for DSPE-PEG systems, as clearly illustrated in Figure 1. The finding indicates that the possible assignment is either to micellar- or DSPE-specific processes. As shown in Figure 3b, if we re-plot $\Delta\epsilon_1$ as a function of the molar concentration of the DSPE-PEGs, the data for different M_{PEG} perfectly collapse on the same straight line. Thus, this relaxation has to be assigned to the rotation of the charged DSPE head group. This interpretation is well supported by the data of Katzee et al.[24] A slightly larger τ_1 for higher M_{PEG} may reflect the stronger frictional forces for head group rotation with longer PEG chains.

3.2. Hydration of DSPE-PEG Micelles. Using the experimentally obtained bulk-water amplitude, $\Delta\epsilon_3$, we estimated the effective hydration number of the DSPE-PEG molecule and that for the corresponding PEG.

The generalized Cavell equation[25]

$$\Delta\epsilon_i = \frac{\epsilon}{3(\epsilon + (1-\epsilon)A_i)} \frac{N_A}{k_B T \epsilon_0} \frac{g_i \mu_{Gi}^2}{(1-\alpha_i f_i)^2} c_i \qquad (8)$$

connects the relaxation amplitude of the ith process, $\Delta\epsilon_i$, to the concentration of the relaxation species, c_i, where μ_{Gi} is a gas-phase dipole moment, α_i a polarizability, f_i the field factor, A_i

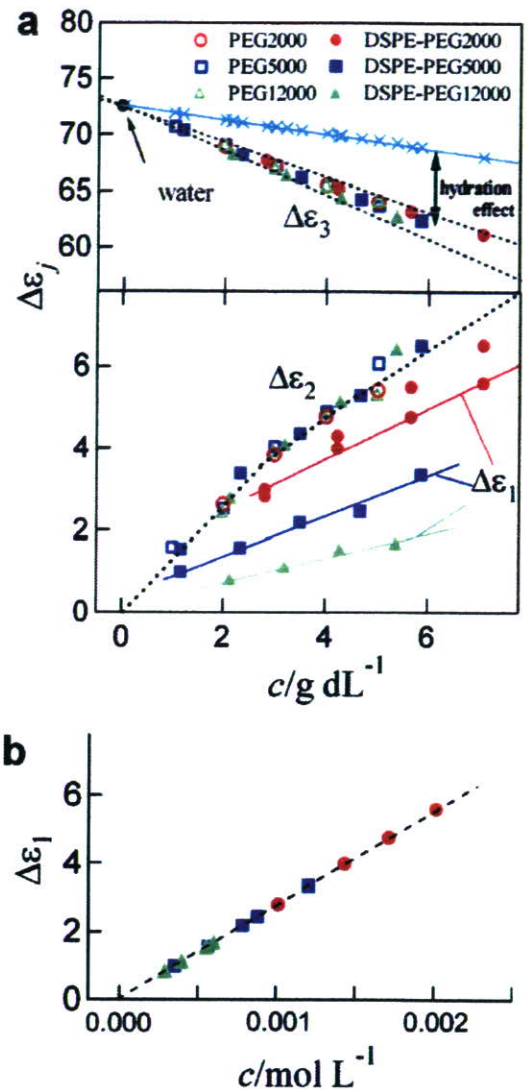

Figure 3. The relaxation amplitudes for aqueous solutions of DSPE-PEG and normal PEG with M_{PEG} = 2000, 5000, and 12 000 at 25 °C as a function of polymer concentration in g dL^{-1} (a) and $\Delta\epsilon_1$ replotted as a function of molar concentration of DSPE-PEG (b). A light blue colored solid line shown together with $\Delta\epsilon_3$ in panel a represents the ideal bulk-water amplitude calculated from analytical water concentration under the assumption that all water molecules in solution contribute to the bulk-water process with the same Kirkwood dipole−dipole orientational correlation factor as pure water.

the shape parameter of the reaction field, ϵ the static permittivity, g_i the dipole−dipole correlation factor, k_B the Boltzmann constant, N_A the Avogadro's number, and ϵ_0 the vacuum permittivity.

Equation 8, normalized to pure water, yields the apparent water concentration at polymer concentration c, $c_w^{app}(c)$, as

$$c_w^{app}(c) = c_w(c)\frac{g_w(c)}{g_w(0)} = \frac{\epsilon(0)(2\epsilon(c)+1)}{\epsilon(c)(2\epsilon(0)+1)} \frac{(1-\alpha_w f_w(c))^2}{(1-\alpha_w f_w(0))^2} \frac{\Delta\epsilon_w(c)}{\Delta\epsilon_w(0)} c_w(0) \qquad (9)$$

where $\Delta\epsilon_w(0) = 72.5$ and $\Delta\epsilon_w(c) = \Delta\epsilon_3(c)$. Assuming a spherical water molecule ($A_i = 1/3$) having a radius $r = 0.1425$

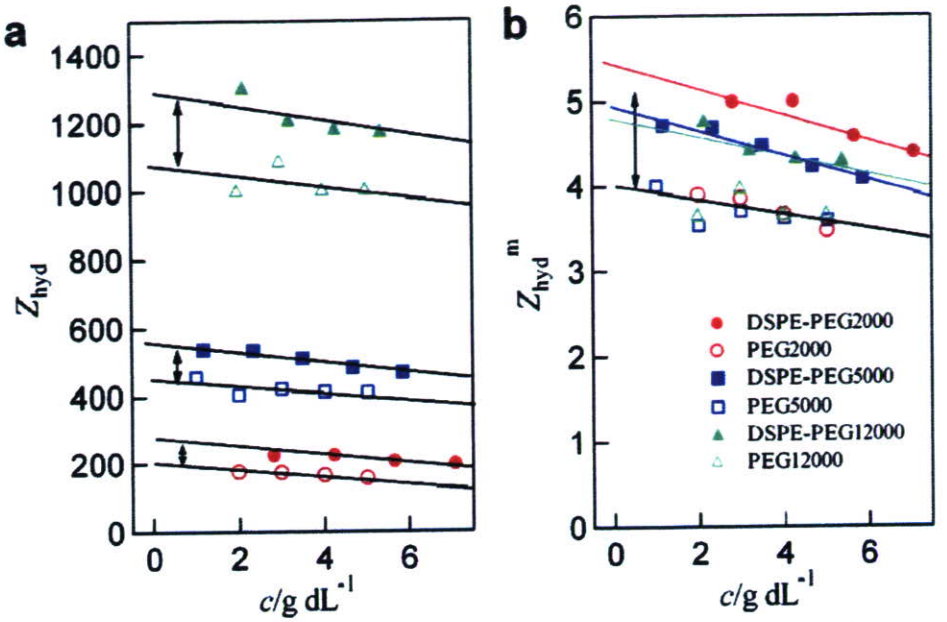

Figure 4. The effective hydration number of DSPE-PEG and PEG molecules, Z_{hyd} (a), and those per ethylene glycol monomer unit, Z_{hyd}^m (b), as a function of polymer concentration, c. These quantities are calculated from the concentration dependence of the dispersion amplitude of the bulk-water process, $\Delta\epsilon_3$. Z_{hyd} explains the number of water molecules that cannot contribute to the bulk-water process due to the hydration effects.

nm and a polarizability $\alpha_w = 1.607 \times 10^{-40}$ Cm^2/V, the apparent concentration of bulk water, $c_w^{app}(c)$, i.e., the concentration of water molecules contributing to the bulk-water relaxation process, can be deduced. We define the effective hydration number of a polymer molecule, Z_{hyd}, or that per PEG monomer unit, Z_{hyd}^m, by converting the difference between the apparent water concentration, $c_w^{app}(c)$ and analytical water concentration, $c_w(c)$, to the corresponding number of water molecules per DPSE-PEG molecule

$$Z_{hyd} = [c_w(0) - c_w^{app}(c)]/c \qquad (10)$$

or that per EG monomer unit, $Z_{hyd}^m = Z_{hyd}/N$, where N is the degree of polymerization of PEG. According to the definition, using the magnitude of polarization fluctuations as a suitable measure, Z_{hyd} gives the number of water molecules that cannot contribute to the bulk-water relaxation process due to the hydration effects, which significantly slow down their intermolecular collective dynamics.

In Figure 4, Z_{hyd} and Z_{hyd}^m are plotted as a function of c. Z_{hyd} for all the investigated solutions seems to be a gradually decreasing function of c, giving the Z_{hyd}^m value of 5.0−5.5 ($c \to 0$) for all DSPE-PEGs and ~4 ($c \to 0$) for the corresponding PEGs as shown in Figure 4b. This demonstrates that approximately 5.0−5.5 hydrated water molecules per EG unit are as tightly bound as they show significant slowing down and consequently lose the nature of bulk water. The systematically higher Z_{hyd} values for DSPE-PEG than those for the corresponding normal PEG indicate that the difference is not likely to be related simply to the additional hydration water to the DSPE charged head group. If the difference of Z_{hyd} values was solely attributed to the hydration of the phosphatidylethanolamine group, the effect should become less pronounced with increasing M_{PEG} due to relatively smaller contribution of the DSPE head group hydration compared to dominating long-chain PEG hydration. However, we can see the significant difference, ~200, for $M_{PEG} = 12\,000$, well within the accuracy of our DRS experiments/analysis. Also, a hydration number of ~200 for phosphatidylethanolamine group would be too large to be accommodated around the phosphatidylethanolamine group. Therefore, we conclude that not only excess hydration water molecules to the DSPE charged head group, but packing effects of PEG into a micellar structure also contribute to higher Z_{hyd} values for DSPE-PEG than those for normal PEG.

Direct numerical comparison of Z_{hyd} with literature values is rather restricted because of the lack of appropriate references. However, NMR studies of Nilsson and Lindman on poly(oxyethylene) alkylether (often abbreviated as C_iE_j) in D_2O yielded hydration numbers in the range of 5 to 6 from the translational self-diffusion constant of D_2O.[37] Recently, Schrödle et al.[20] made an extensive dielectric study on aqueous $C_{12}E_5$, for both aqueous micellar and liquid crystalline phases and obtained about 3.5 to 4.0 bound water molecules per ethylene glycol (EG) monomer unit for micellar soultions. Using DRS also, Sato et al. reported that, for aqueous poly(oxyethylene) cholesteryl ether (ChE_j with $j = 10$ and 15), each oxyethylene unit is hydrated by approximately 4 to 4.5 water molecules at ambient condition.[21] The latter evaluation is in better agreement with the present Z_{hyd}^m for the DSPE-PEGs. Apparently, there is some dependence of the oxyethylene group hydration on the chain length j for short-chain PEGs in surfactants. The present results on DSPE-PEG solutions also fit into the existing set of PEG hydration numbers. Besides the contribution of direct phosphatidylethanolamine group hydration, the slightly higher hydration number possibly reflects a different packing of DSPE-PEG molecules into the micelles compared to C_iE_j surfactants. The present Z_{hyd}^m for normal PEGs is comparable with the recent estimation of Shikata et al.[22] by DRS on aqueous poly(ethylene oxide)s.

Anyway, for sufficiently long oxyethylene chains, on average 4−5 water molecules are hydrated per EG monomer unit irrespective of the type of hydrophobic group, and this number

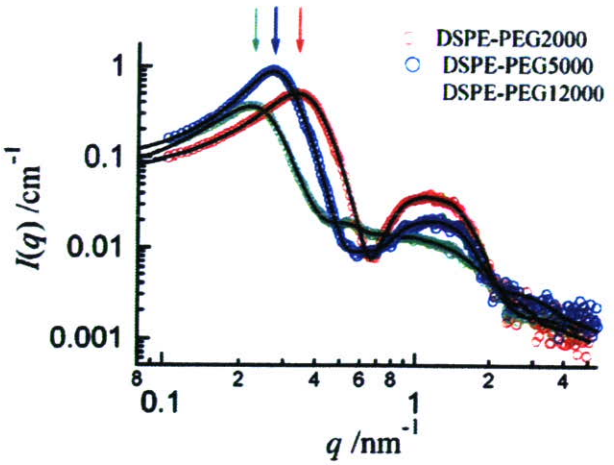

Figure 5. The absolute X-ray scattered intensities $I(q)$ of the aqueous DSPE-PEG solutions with $M_{PEG} = 2000$, 5000, and 12 000 at $W_{DSPE-PEG}$ (weight fraction of DSPE-PEG) = 0.04 at 25 °C. The arrows indicate the intermicellar correlation peak positions q^*, where the distance $d^* = 2\pi/q^*$ gives a measure of center-of-mass to center-of-mass distance of the micelles.

may be almost universal for all PEG-based surfactant systems. Namely, the hydration of the PEG chain is basically governed by the hydration of each EG monomer, and the total hydration number of a polymer or a micelle is approximately given by the simple sum of hydrated water molecules to each EG monomer unit. These hydrated water molecules must contribute to the compressibility of the system and repulsive interaction between the micelles inducing steric hindrance effect.

3.3. The Static Structures of DSPE-PEG Micelles. Figure 5 shows the (collimation-corrected) absolute X-ray scattered intensities $I(q)$ for the aqueous solutions of DSPE-PEG with $M_{PEG} = 2000$, 5000, and 12 000, respectively, at a weight fraction of DSPE-PEG, $W_{DSPE-PEG} = 0.04$. The experimental $I(q)$ of all DSPE-PEG solutions clearly shows the typical features of a scattering function from globular particles. The scattering vector q^*, corresponding to the apparent low-q peak position in $I(q)$, provides a semiquantitative estimation of the averaged intermicellar (i.e., center-of-mass to center-of-mass) distance d^* without imposing any interaction potential model. If we simply extend the idea of Bragg reflections, d^* is approximated as $2\pi/q^*$. As we will show later using a quantitative $S(q)$ analysis, this leads to a small systematic overestimation of d^*. As highlighted by arrows, q^* is shifted to lower-q values with rising M_{PEG}, resulting in $d^* = 19$, 24, and 28 nm, respectively, for $M_{PEG} = 2000$, 5000, and 12 000. To extract more specific information about the micellar structure (size, shape, and internal core−shell structure) as well as the intermicellar interaction potentials, we need further quantitative analysis of the scattering functions. As will be shown below, the GIFT technique[21,30−36] offers an excellent route to access to these quantities.

The SAXS data for aqueous DSPE-PEG solutions were analyzed by the generalized indirect Fourier transformation (GIFT) technique. $P(q)$ and $S(q)$ were simultaneously determined, leaving $P(q)$ model-free, whereas the choice of a plausible interaction potential model and an appropriate closure relation were necessary for $S(q)$. In Figure 6, we display the results of the GIFT analysis.

Within the framework of the mean-spherical approximation (MSA),[38] the direct correlation function $c(r)$ is related to the particle potential $v(r)$ as

$$c(r) = -\beta\, v(r) \tag{11}$$

where $\beta = 1/k_BT$. $S(q)$ for aqueous DSPE-PEG solutions is calculated assuming a screened Coulomb (Yukawa) potential

$$\begin{aligned} \beta\, v(r) &= \frac{Z_{eff}^{\,2} e_0^{\,2}}{4\pi\epsilon\epsilon_0 k_B T} \cdot \frac{e^{-\kappa(r-\sigma)}}{r(1+\kappa\sigma/2)^2} & r > \sigma \\ &= \infty & r < \sigma \end{aligned} \tag{12}$$

where e_0 is the elementary charge, Z_{eff} the effective charge number of the particle, σ the hardsphere diameter, and ϵ the static dielectric constant of the solvent. When there is no salt added, the reciprocal Debye screening length κ is determined by

$$\kappa^2 = \frac{e_0^{\,2}}{\epsilon\epsilon_0 k_B T} n Z_{eff} \tag{13}$$

where n is the number density of the particle, and nZ_{eff} is the net charge of released counter ions in unit volume. We numerically solved the Ornstein−Zernike (OZ) equation[39]

$$h(r) = c(r) + n \int d\mathbf{r}'\, c(|\mathbf{r} - \mathbf{r}'|)\, h(\mathbf{r}') \tag{14}$$

by employing the Rogers−Young[40] (RY) closure relation

$$g(r) = e^{-\beta v(r)}\left\{1 + \frac{1}{f(r)}[e^{f(r)(h(r)-c(r))} - 1]\right\} \tag{15}$$

where $f(r) = 1 - \exp(-\alpha r)$ is the mixing function. When $\alpha \to 0$ and $\alpha \to \infty$, RY coincides respectively with Percus−Yevick[41] (PY) and hypernetted chain (HNC). The mixing parameter is adjusted so as to attain the self-consistency of the thermodynamic parameters calculated via the fluctuation root and the virial root.

In Figure 7, the pair-distance distribution functions, $p(r)$, for the DSPE-PEG micelles are shown, where $p(r)$ was obtained as an inverse Fourier transformation of $P(q)$. From the r-value at which $p(r)$ goes to zero, the total diameter of the DSPE-PEG micelle, the so-called D_{max}, is obtained. The low-r local maximum and minimum in $p(r)$ come essentially from the convolution of the negative and positive electron density fluctuations, respectively, of the hydrophobic core and hydrophilic shell of the micelles. It is well-established that, even when these local maximum and minimum do not clearly show up but only appear as a low-r bump due to a relatively good contrast of the core−shell structure, the distance corresponding to the inflection point located on the higher-r side of the local minimum gives a semiquantitative measure of the hydrophobic core diameter, D_C. This holds even when the micelle is highly elongated. Furthermore, the distance between the local maximum and minimum almost universally coincides with $D_C/2$, so that this point can provide a semiquantitative measure of the core radius, r_C. Accordingly, we found that, for all the investigated DPSE-PEG solutions, the deduced D_C and r_C are 5.0 and 2.5 nm, respectively, which is virtually independent of M_{PEG}. Taking molecular volumes from literatures,[42,43] the partial volume of the hydrocarbon group of DSPE, V_{hc}, is calculated as $V_{hc} = 1.016$ nm.[3] If we estimate the aggregation number of DSPE-PEG molecules into micellar structure, according to $N_{agg} = 4\pi r_c^3/3V_{hc}$, we obtain $N_{agg} \sim 72$. This estimation may involve about 10% of error due to spatial resolution of our SAXS measurements and analysis, but the N_{agg} value is very close to the aggregation number of about 75 for DSPE-PEG2000 and DSPE-PEG5000 obtained by static light scattering (SLS) experiments in the pioneer work of Jonsson et al.[14]

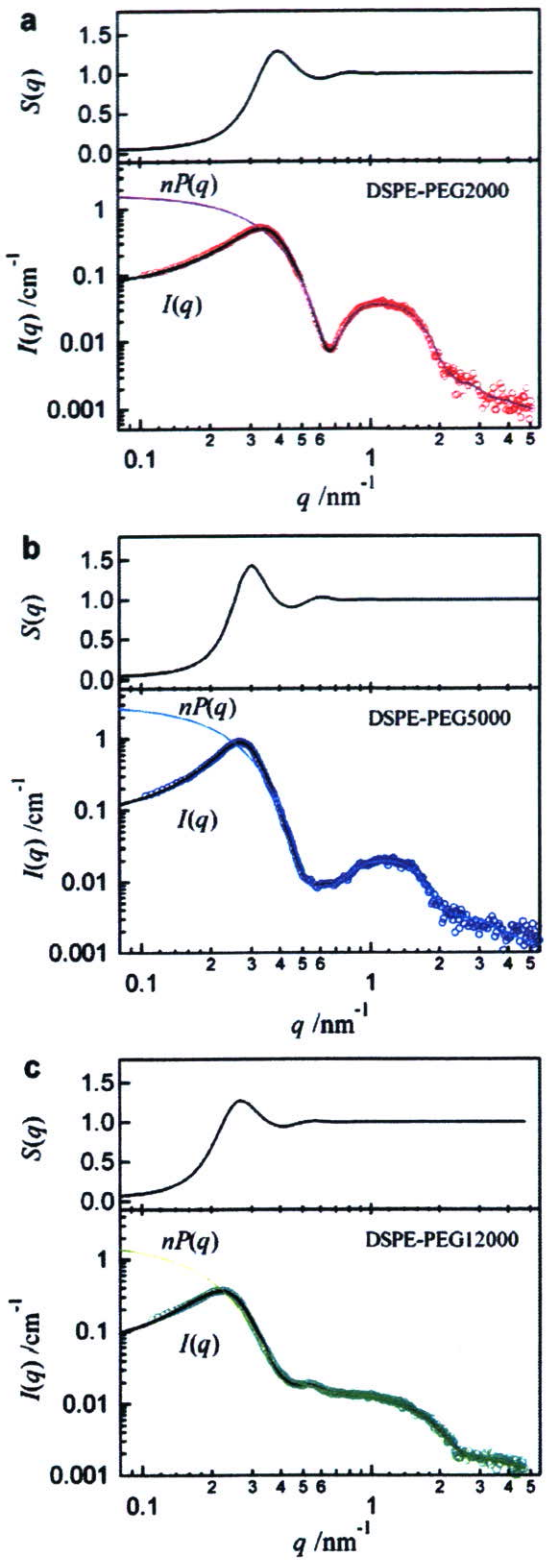

Figure 6. GIFT analysis of the X-ray scattered intensities $I(q)$ of aqueous DSPE-PEG solutions at $W_{DSPE-PEG} = 0.04$ at 25 °C for M_{PEG} = 2000 (a), 5000 (b), and 12 000 (c). Black solid and colored solid curves in the lower panel represent GIFT fit to $I(q)$ and the calculated form factor for n particles existing in unit volume, $nP(q)$, respectively. Also shown in the upper panel is the static structure factor $S(q)$ calculated assuming a screened Coulomb (Yukawa) potential model and Rogers−Young (RY) closure relation.

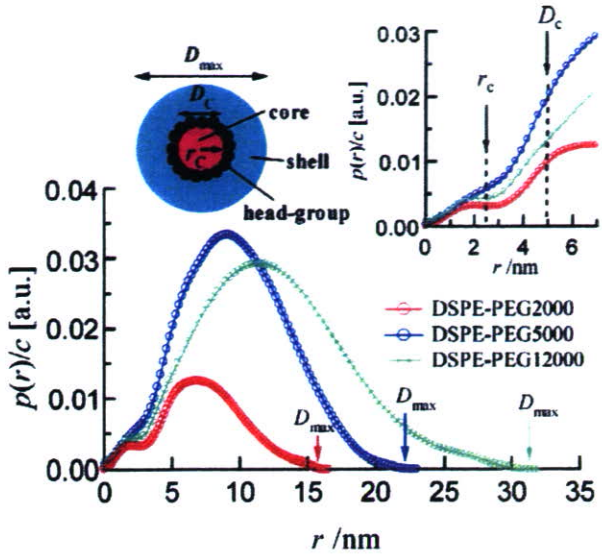

Figure 7. Particle characterization of the DSPE-PEG micelles. The normalized pair-distance distribution functions by polymer molar concentration, $p(r)/c$, for aqueous DSPE-PEG solutions with M_{PEG} = 2000, 5000, and 12 000 at $W_{DSPE-PEG} = 0.04$. The enlarged view in the low-r region is also presented in the inset. The two inflection points in $p(r)$ highlighted by two arrows can be the prominent measure of the core radius, r_c, and diameter, D_c, from which $r_c = 2.5 \pm 0.1$ nm is deduced for all M_{PEG}. This implies nearly identical aggregation numbers for all DSPE-PEG micelles despite the considerable variation of hydrophilic PEG chain length.

Figure 8 presents the number of water molecules existing in different states when involved into a DSPE-PEG micelle and the resulting fraction, ϕ_{bulk}, of the micelle volume occupied by bulk water. The difference between the total number of water molecules exiting in the micelle (per DSPE-PEG molecule), Z_{mic}^{m}, estimated from micellar geometry, and the effective hydration number of a DSPE-PEG molecule, Z_{hyd}^{m}, provides the number of water molecules that still preserve the nature of bulk water, despite penetrating the area of the PEG hydrophilic groups of the micellar structure. Those water molecules are situated in the region $r_C < r < D_{max}/2$ from the center of micelle. ϕ_{bulk} is calculated as $\phi_{bulk} = 1 - [N_{agg}(V_{DSPE-PEG} + V_{hyd})]/V_{mic}$, where $V_{mic} = 4\pi(D_{max}/2)^3/3 = \pi D_{max}^3/6$ is the micellar volume. V_{hyd} is the volume occupied by the water molecules hydrated to a DSPE-PEG molecule, deduced from DRS as shown in Figure 4a, and $V_{DSPE-PEG}$ is the molecular volume of DSPE-PEG. N_{agg} is fixed to 72.

The combined DRS/SAXS analysis clearly reveals that, as shown in the upper panel of Figure 8, a significant amount of water molecules residing inside the head group area of the micelle, indeed reaching 60−75% volume of the total volume of the micelle, still preserves the nature of bulk water. This means that the interpretation of the structure of DSPE-PEG micelles as perfect charged hard spheres (HS) of diameter D_{max} is obviously too simplified. The pronounced increase of ϕ_{bulk} with increasing M_{PEG} demonstrates that more "diluted" or compressible micelles are formed for longer PEG chains, which are essentially stretched. With increasing M_{PEG}, such an open structure will allow easier mutual penetration or overlap of the hydrated PEG layers of approaching micelles.

In Figure 9, we display the pair-correlation functions $g(r)$ for the DSPE-PEG micelles, which are deduced from $S(q)$ analysis of the GIFT procedure. In view of the above results, it is certainly not possible to reproduce SAXS data of the DSPE-PEG solutions using a hard sphere (HS) interaction potential

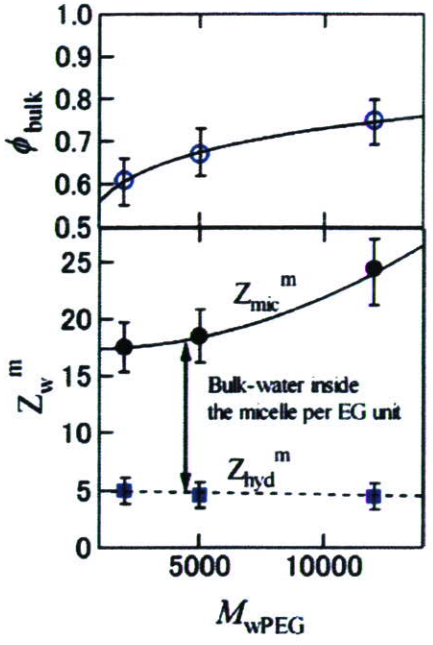

Figure 8. The amount of water molecules in different states involved into a DSPE-PEG micelle for different M_{PEG} as obtained by SAXS and DRS. The lower panel shows the total number of water molecules per EG monomer, Z_{mic}^m, that reside within the micelle (i.e., for $r < D_{max}/2$) according to SAXS, and the effective hydration number per EG unit, Z_{hyd}^m, of a DSPE-PEG molecule deduced from DRS. Because Z_{hyd}^m represents the number of tightly bound, thus slowly relaxing water molecules, the difference between Z_{mic}^m and Z_{hyd}^m gives the number of "bulk-water" molecules (per EG monomer) in the micelle, Z_{bulk}^m. The upper panel displays the resulting fraction, ϕ_{bulk}, of the micelle volume occupied by bulk water.

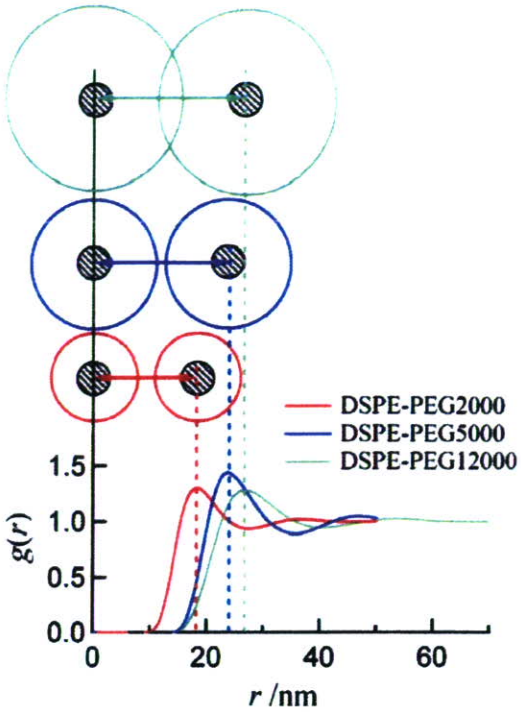

Figure 9. The pair-correlation functions $g(r)$ for the DSPE-PEG micelles (M_{PEG} = 2000, 5000, and 12 000) in water at $W_{DSPE-PEG}$ = 0.04 as obtained by GIFT analysis of SAXS intensities $I(q)$, assuming a screened Coulomb (Yukawa) potential and the Rogers−Young (RY) closure relation. On the same spatial scale, the schematic picture of the micelles is drawn to visualize the interplay between the intermicellar (average) distance and the micellar geometry, where the shaded circle represents a hydrophobic core having $r_c \sim 2.5$ nm.

model for $S(q)$. Although we found that the shape of $S(q)$ can be approximated by a screened Coulomb (Yukawa) potential, one has to recognize that the produced $S(q)$ parameters cannot necessarily be exact. The major reason is that the charges of the DSPE head groups are not on the surface of micelles but are highly localized close to the hydrophilic/hydrophobic interface, whereas the total size of the micelles is far bigger than that of the effective charged sphere, consisting of a hydrophobic core and charged head groups. Furthermore, we cannot exactly define the static dielectric constant of the hydrated PEG layer due to its definition as a macroscopic quantity. However, its anticipated lower (effective) value compared to pure water will give rise to a larger strength but shorter screening length for the electrostatic repulsion between the effective charged spheres than one would obtain when the charged spheres were directly put into water. Of course, the excluded volume effect caused by DPSE-PEG polymers in themselves and hydrated water molecules also greatly contribute to the intermicellar repulsive interaction and osmotic compressibility of the systems. Therefore, it is apparent that a DSPE-PEG micelle cannot be treated as an ideal charged colloid in water. Nevertheless, the extracted g(r), shown in Figure 9, provides an intuitive picture of spatial correlations of these micelles, giving insights into the interplay between the intermicellar distance and the micellar geometry. Note that the pronounced peak positions in $g(r)$ more or less coincide with d^* obtained with a potential model-free approach; see Figure 5. This indicates that the discussion made here is not biased by an approximate modeling of $S(q)$.

At the investigated concentrations, an overlap and interpenetration of hydrated PEG layers eventually occur among DSPE-PEG12000 micelles, whereas a direct contact of micelles hardly takes place for DSPE-PEG2000 and DSPE-PEG5000. Owing to the low ionic strength and the relatively small micellar radii of DSPE-PEG2000 and DSPE-PEG5000, long-range electrostatic repulsion is strong enough to keep the relatively small micelles apart. Figure 9 reveals that at low ionic strength both an electrostatic repulsion induced by the charged head group and an excluded volume effect of the hydrated PEG layer contribute to the net repulsive interaction among the PEG-lipid micelles, which must be an essential factor for the function of PEG-lipids as a stabilizer of liposomes. It is naturally anticipated that, at higher ionic strength, such as a physiological condition, the steric hindrance induced by hydrated PEG chains becomes more and more dominant over the efficiently screened electrostatic repulsion for the interparticle repulsive interaction of PEG-lipid micelles. We consider that the main conclusion of Jonsson et al.[14] (that the electrostatic intermicellar interactions are of minor importance for the PEG-lipid micelles compared to the repulsive forces from the steric interaction from the overlap of PEG layers) arose from the fact that all their experiments were made in 150 mM NaCl solutions. To clarify this aspect, we plan to investigate further the effect of ionic strength of solvent on the repulsive interactions of DSPE-PEG micelles. From the methodological point of view, the DRS/SAXS approach will be applicable to detailed physicochemical analyses of PEG-conjugated proteins, such as PEG-Hb and PEG-albumin.[44]

4. Conclusions

We have carried out SAXS and DRS experiments on aqueous solutions of PEG-conjugated phospholipid (DSPE-PEG) with

different M_{PEG} = 2000, 5000, and 12 000 Da. The results have provided deep physical insights into hydration and static structures of the DSPE-PEG micelles. The complex dielectric spectra of these solutions exhibit typical multistep relaxation behavior, the three relaxation processes centered at ~0.1, ~5, and ~19 GHz, being respectively assigned to the charged DSPE head group rotation, cooperative molecular motions in hydrated PEG layers, and cooperative hydrogen-bond network rearrangement dynamics of bulk water. A quantitative analysis of the bulk-water amplitude based on Cavell theory yields the effective hydration number of a DSPE-PEG molecule, $Z_{hyd} \sim 5.0$ (per ethylene oxide monomer unit), which turns out to be virtually independent of M_{PEG}. Although the extracted Z_{hyd} for DSPE-PEG, exceeding that for normal PEG by ca. 20%, involves inseparable effects of the DSPE charged head group hydration and packing of PEG chains into micellar structure, the finding clearly indicates that the hydration of PEG chains is mainly governed by the hydration of each EG monomer. In view of the pair-distance distribution functions, $p(r)$, deduced by the GIFT evaluation of the SAXS intensity distributions, the DSPE-PEGs produce nearly spherical micelles in aqueous environment, whose maximum diameters are estimated to be ~16, 22, and 31 nm, respectively, for M_{PEG} = 2000, 5000, and 12 000. The volume of DSPE-PEG and hydrated water molecules only accounts for 30−40% of the total micellar volume; the remaining more than 60% is occupied by bulk-like water. The structure factor $S(q)$ analysis unambiguously demonstrates that, at low ionic strength, both electrostatic repulsion induced by the charged head group and excluded volume effects of the hydrated PEG layer, significantly contribute to the net repulsive interaction among the PEG-lipid micelles, which should be a key factor for the function of PEG-lipids as a stabilizer of liposomes. Our finding does not necessarily support the generally accepted view that only the latter, excluded volume effect of hydrated PEG chains, is of major importance for the repulsive forces acting on PEG-lipid micelles. This will hold only at high ionic strength.

Acknowledgment. This work was supported in part by Health Sciences Research Grants (Research on Regulatory Science of Pharmaceuticals and Medical Devices), from the Ministry of Health, Labour, and Welfare, Japan, and Grants-in-Aid for Young Scientists (B) (No. 18740264) from the Ministry of Education, Culture, Sports, Science, and Technology (MEXT), Japan. T.S. acknowledges supports from the 21st century COE program at Waseda University funded by MEXT. The authors thank Alexander Stoppa for providing interferometer data of DSPE-PEG and PEG solutions. Professor Kenji Aramaki and late Professor Hironobu Kunieda are gratefully appreciated for their kind help for SAXS measurements. Some of the PEG-derivatives were kindly provided by NOF Co.

References and Notes

(1) Chandler, D. *Nature* **2005**, *437*, 640.
(2) Bangham, A. D.; Horne, R. W. *J. Mol. Biol.* **1964**, *12*, 660.
(3) Torchilin, V. P. *Nat. Rev. Drug Discovery* **2005**, *4*, 145.
(4) Klibanov, A. L.; Maruyama, K.; Torchilin, V. P.; Huang, L. *FEBS Lett.* **1990**, *268*, 235.
(5) Yoshioka, H. *Biomaterials* **1991**, *12*, 861.
(6) Mobed, M.; Chang, T. M. S. *Biomaterials* **1998**, *19*, 1167.
(7) Tsuchida, E., Ed. *Blood Substitutes, Present and Future Perspectives*; Elsevier Science S.A.: Lausanne, Switzerland, 1998.
(8) Sakai, H.; Tomiyama, K. I.; Sou, K.; Takeoka, S.; Tsuchida, E. *Bioconjugate Chem.* **2000**, *11*, 425.
(9) Sou, K.; Endo, T.; Takeoka, S.; Tsuchida, E. *Bioconjugate Chem.* **2000**, *11*, 372.
(10) Sakai, H.; Tsai, A. G.; Kerger, H.; Park, S. I. Takeoka, S.; Nishide, H.; Tsuchida, E.; Intaglietta, M. *J. Biomed. Mater. Res.* **1998**, *40*, 66.
(11) Sakai, H.; Takeoka, S.; Park, S. I.; Kose, T.; Nishide, H.; Izumi, Y.; Yoshizu, A.; Kobayashi, K.; Tsuchida, E. *Bioconjugate Chem.* **1997**, *8*, 23.
(12) Sou, K.; Klipper, R.; Goins, B.; Tsuchida, E.; Phillips, W. T. *J. Pharmacol. Exp. Ther.* **2005**, *312*, 702.
(13) Kenworthy, A. K.; Hristova, K.; Needham, D.; McIntosh, T. J. *Biophys. J.* **1995**, *68*, 1921.
(14) Johnsson, M.; Hansson, P.; Edwards, K. *J. Phys. Chem. B* **2001**, *105*, 8420.
(15) Koynova, R.; Tenchov, B.; Rapp, G. *Colloids Surf., A* **1999**, *149*, 571.
(16) Buchner, R.; Barthel, J. *Annu. Rep. Prog. Chem., Sect. C: Phys. Chem.* **2001**, *97*, 349.
(17) Fukasawa, T.; Sato, T.; Watanabe, J.; Hama, Y.; Kunz. W.; Buchner, R. *Phys. Rev. Lett.* **2005**, *95*, 197802.
(18) Sato, T.; Buchner, R. *J. Phys. Chem. A* **2004**, *108*, 5007.
(19) Sato, T.; Buchner, R. *J. Chem. Phys.* **2003**, *119*, 10789.
(20) Schrödle, S.; Hefter, G.; Kunz, W.; Buchner, R. *Langmuir* **2006**, *22*, 924.
(21) Sato, T.; Hossain, M. d. K.; Acharya, D. P.; Glatter, O.; Chiba, A.; Kunieda, H. *J. Phys. Chem. B* **2004**, *108*, 12927.
(22) Shikata, T.; Takahashi, R.; Sakamoto, A. *J. Phys. Chem. B* **2006**, *110*, 8941.
(23) Fernandez, P.; Schrödle, S.; Buchner, R.; Kunz, W. *ChemPhysChem* **2003**, *4*, 1065.
(24) Kaatze, U.; Gopel, K.-D.; Pottel, R. *J. Phys. Chem.* **1985**, *89*, 2565.
(25) Barthel, J.; Hetzenauer, H.; Buchner, R. *Ber. Bunsen Ges.* **1992**, *96*, 1424.
(26) Barthel, J.; Bachhuber, K.; Buchner, R.; Hetzenauer, H.; Kleebauer, K. *Ber. Bunsen Ges.* **1991**, *95*, 853.
(27) Glatter, O.; Kratky, O. *Small-Angle X-ray Scattering*; Academic: London, 1982.
(28) Lindner, P.; Zemb, Th., Eds. *Neutron, X-Ray and Light Scattering*; North-Holland: Amsterdam, 1991.
(29) Glatter, O. *J. Appl. Crystallogr.* **1997**, *10*, 415.
(30) Strey, R.; Glatter, O.; Schubert, K. -V.; Kaler, E. W. *J. Chem. Phys.* **1996**, *105*, 1175.
(31) Shrestha, L. K.; Sato, T.; Acharya D. P.; Iwanaga, T.; Aramaki, K.; Kunieda, H. *J. Phys. Chem. B* **2006**, *110*, 12266.
(32) Brunner-Popela, J.; Glatter, O. *J. Appl. Crystallogr.* **1997**, *30*, 431.
(33) Weyerich, B.; Brunner-Popela, J.; Glatter, O. *J. Appl. Crystallogr.* **1999**, *32*, 197.
(34) Orthaber, D.; Bergmann, A.; Glatter, O. *J. Appl. Crystallogr.* **2000**, *33*, 218.
(35) Bergmann, A.; Orthaber, D.; Scherf, G.; Glatter, O. *J. Appl. Crystallogr.* **2000**, *33*, 869.
(36) Fritz, G.; Bergmann, A.; Glatter, O. *J. Chem. Phys.* **2000**, *113*, 9733.
(37) Nilsson, P. G.; Lindman, B. *J. Phys. Chem.* **1983**, *87*, 4756.
(38) Hayter, J. B.; Penfold, J. *Mol. Phys.* **1981**, *42*, 109.
(39) Ornstein, L. S.; Zernike, F. *Proc. Sect. Sci. K. Ned. Akad. Wet.* **1914**, *17*, 793.
(40) Rogers, F. J.; Young, D. A. *Phys. Rev. A* **1984**, *30*, 999.
(41) Percus, J. K.; Yevick, G. J. *Phys. Rev.* **1958**, *110*, 1.
(42) Nagle, J. F.; Tristram-Nagle, S. *Biochim. Biophys. Acta* **2000**, *1469*, 159.
(43) Nagarajan, R.; Ruckenstein, E. *Langmuir* **1991**, *7*, 2934.
(44) Manjula, B. N.; Tsai, A.; Upadhya, R.; Perumalsamy, K.; Smith, P. K.; Malavalli, A.; Vandegriff, K.; Winslow, R. M.; Intaglietta, M.; Prabhakaran, M.; Friedman, J. M.; Acharya, A. S. *Bioconjugate Chem.* **2003**, *14*, 464.

ARTICLE IN PRESS

Available online at www.sciencedirect.com

ScienceDirect

Biomaterials

ELSEVIER

Biomaterials ▮ (▮▮▮▮) ▮▮▮–▮▮▮

www.elsevier.com/locate/biomaterials

Selective uptake of surface-modified phospholipid vesicles by bone marrow macrophages *in vivo*

Keitaro Sou[a], Beth Goins[b], Shinji Takeoka[a], Eishun Tsuchida[a,*], William T. Phillips[b]

[a]*Advanced Research Institute for Science and Engineering, Waseda University, Tokyo 169-8555, Japan*

[b]*Department of Radiology, University of Texas Health Science Center at San Antonio, 7703 Floyd Curl Drive, San Antonio, TX 78229-3900, USA*

Received 29 August 2006; accepted 31 January 2007

Abstract

An advantage of using vesicles (liposomes) as drug delivery carriers is that their pharmacokinetics can be controlled by surface characteristics, which can permit specific delivery of the encapsulated agents to organs or cells *in vivo*. Here we report a vesicle formulation which targets the bone marrow after intravenous injection in rabbits. Surface modification of the vesicle with an anionic amphiphile; L-glutamic acid, *N*-(3-carboxy-1-oxopropyl)-, 1,5-dihexadecyl ester (SA) results in significant targeting of vesicles to bone marrow. Further incorporation of as little as 0.6 mol% of poly(ethylene glycol)-lipid (PEG-DSPE) passively enhanced the distribution of SA-vesicles into bone marrow and inhibited hepatic uptake. In this model, more than 60% of the intravenously injected vesicles were distributed to bone marrow within 6 h after administration of a small dose of lipid (15 mg/kg b.w.). Histological evidence indicates that the targeting was achieved due to uptake by bone marrow macrophages (BMMϕ). The efficient delivery of encapsulated scintigraphic and fluorescent imaging agents to BMMϕ suggests that vesicles are promising carriers for the specific targeting of BMMϕ and may be useful for delivering a wide range of therapeutic agents to bone marrow.

Keywords: Nanoparticle; Liposome; Bone marrow; Macrophage; Drug delivery; Surface modification

1. Introduction

Nanoparticulate carrier systems have been investigated as candidates for targeted delivery in cancer therapy and gene therapy [1,2]. A wide variety of nanoparticle systems have been developed for biological applications. One of the advantages of using nanoparticulate materials is based on their controllable surface properties which permit specific interactions with cells, tissues, and organs. Although a number of investigators have demonstrated that endocytosis of nanoparticles *in vitro* is accelerated by surface modification of the particles with specific ligands, the specific *in vivo* targeting of cells remains challenging because it is hindered by competing interactions, especially fairly high mononuclear phagocyte system (MPS) uptake *in vivo*.

Phospholipid vesicles (liposomes) have been widely investigated as potential carriers for drugs, genes, and proteins because their capsular structure permits encapsulation of various therapeutic agents [2–4]. Because of their particulate nature, these vesicles are trapped in the MPS, particularly hepatic Kupffer cells and spleen macrophages following intravenous administration [5,6]. Once in the bloodstream, the binding of plasma proteins such as immunoglobulins, complement proteins, apolipoproteins, etc., which together are termed "opsonins" on the vesicular surface have been reported to accelerate phagocytosis of the vesicles by macrophages, because the macrophages have scavenger receptors to bind the opsonins [5]. In addition to this mechanism, vesicles containing anionic phospholipids such as phosphatidylserine (PS), which are markers of apoptotic cells, have been reported to bind with a PS receptor on macrophages [7]. Improved vesicles with

*Corresponding author. Tel.: +81 3 5286 3120; fax: +81 3 3205 4740.
E-mail addresses: ksou@waseda.jp (K. Sou), eishun@waseda.jp (E. Tsuchida).

0142-9612/$ - see front matter © 2007 Elsevier Ltd. All rights reserved.
doi:10.1016/j.biomaterials.2007.01.041

Please cite this article as: Sou K, et al. Selective uptake of surface-modified phospholipid vesicles by bone marrow macrophages *in vivo*. Biomaterials (2007), doi:10.1016/j.biomaterials.2007.01.041

prolonged circulation times preventing MPS uptake have been formulated with poly(ethylene glycol) (PEG) derivatives [8]. These vesicles have been termed as stealth liposomes, due to their ability to evade uptake by the macrophage, particularly Kupffer cells. Long circulating liposomes with PEG surface modification are currently being used as anti-cancer drug delivery agents [9].

On the other hand, the phagocytic ability of the MPS contributes to achieving an active targeting of particulate carriers to macrophages [10,11]. Macrophages produce a wide range of biologically active molecules that are both beneficial and detrimental. Many of the detrimental effects of macrophages are associated with their pro-inflammatory effects. Thus, interventions targeted to macrophages may open new therapeutic approaches for controlling diseases associated with inflammation. Evidence from a number of sources suggests that cancer-associated inflammation promotes tumor growth and progression, and tumor-associated macrophages play a critical role in the initiation, maintenance, and resolution of inflammation [12]. These tumor-associated macrophages are inactivated by mediators from tumor cells, and they serve to promote tumor growth. The importance of macrophages in disease development has led a number of researchers to investigate methods for the site-specific delivery of drugs to macrophages.

Bone marrow, which contains macrophages, is one of the organs responsible for uptake of circulating particulate materials [5,9,13–17]. Also, macrophages associated with erythroblasts in a hematopoietic environment participate in erythropoiesis control, and engulfment of nuclei from erythroid precursor cells [18,19]. The development of drug delivery systems with specific bone marrow targeting may have therapeutic benefits for hematological malignancies as well as hemopoiesis control. However, very little attention has been paid to bone marrow as part of the MPS because its contribution to the overall MPS is generally much less than that of the liver and spleen *in vivo*. Another essential problem for targeting of BMMϕ is caused by lack of understanding of their specific targeting receptor. Therefore, development of a method for specifically targeting bone marrow will be facilitated by knowledge of the strategies to allow nanoparticles to escape from liver and spleen uptake, but not from bone marrow uptake, and development of specific ligands to induce targeting of bone marrow MPS.

Recently, we have discovered a vesicular formulation which shows remarkable targeting to rabbit bone marrow even when administered at small lipid doses. In this article, we address the components of this vesicle responsible for the targeting of bone marrow and additional vesicular modifications for escaping from liver and spleen uptake, but not from bone marrow. These results may be widely applied to the design of nanoparticulate carriers that target the bone marrow. Bone marrow targeting carriers could open up a wide variety of new therapeutic applications.

2. Materials and methods

2.1. Materials

1,2-Dipalmitoyl-*sn*-glycero-3-phosphocholine (DPPC) and cholesterol (CH) were purchased from Nippon Fine Chemical Co. Ltd. (Osaka, Japan); 1,2-distearoyl-*sn*-glycero-3-phosphoethanolamine-*N*-[monomethoxy poly(ethylene glycol) (5000)] (PEG-DSPE) was purchased from NOF Co. (Tokyo, Japan). L-glutamic acid, *N*-(3-carboxy-1-oxopropyl)-, 1,5-dihexadecyl ester (SA) was synthesized as previously reported [20]. Glutathione was purchased from Sigma (St. Louis, MO). Superoxide dismutase (SOD) was purchased from Wako Pure Chemical Industries Ltd. (Osaka, Japan). 4,4-difluoro-5-methyl-4-bora-3a,4a-diaza-s-indacene-3-dodecanoic acid (C_1-BODIPY C_{12}) and Texas Red (TR) sulfonyl chloride were purchased from Molecular Probes, Inc. (Eugene, OR).

2.2. Preparation of vesicles

All vesicle preparations were performed under sterile conditions. DPPC and CH (1:1 molar ratio), or DPPC, CH, and SA (1:1:0.2 molar ratio) were dissolved in benzene and lyophilized to lipid powders. The mixed lipid powder was hydrated with a glutathione (30 mM) and NaCl (120 mM) solution (pH: 7.0) at 5 g dL^{-1}, and submitted to three cycles of freeze–thawing. After controlling vesicle size by an extrusion method (final pore size of the filter: 0.22 μm, Fuji microfilter, Fuji Photo Film Co., Tokyo, Japan), the unencapsulated glutathione was removed by three ultracentrifugation steps ($3 \times 10^5 g$, 60 min each) and the vesicles were dispersed in saline solution. Surface modification with PEG was performed by making use of the spontaneous incorporation of PEG-DPSE into vesicles [21]. Various concentrations of the PEG-DSPE dispersion were added to the vesicle dispersion and the mixture incubated at 37 °C for 3 h. The vesicle dispersion was ultracentrifuged ($3 \times 10^5 g$, 60 min) to remove unincorporated PEG-DSPE in the supernatant. After washing the precipitated vesicle pellet by ultracentrifugation ($3 \times 10^5 g$, 60 min), the PEG-modified vesicles (PEG-vesicles) were dispersed in saline at 7 g dL^{-1}, and the dispersion was then passed through a sterilized membrane filter (pore size 0.45 μm, DISMIC filter 45, ADVANTEC). The amount of PEG-DSPE incorporated was determined from the peak area ratio of methylene protons of PEG-DSPE (3.63 ppm) to the choline methyl protons of DPPC (3.39 ppm) using ^{1}H-NMR spectroscopy (JEOL JNM-LA500) [21]. SA-vesicles containing 0.3, 0.6, 1.4, and 2.6 mol% of PEG-DSPE on the surface (represented as PEG(0.3)-, PEG(0.6)-, PEG(1.4)-, and PEG(2.6)-[SA-Ve], respectively) and control vesicles containing 2.6 mol% of PEG-DSPE (represented as PEG(2.6)-Ve) were prepared and characterized for these studies. The diameter of the resulting vesicles was determined with a COULTER submicron particle analyzer (N4SD, Coulter, Hialeah, FL), and represented as an average diameter ± standard deviation (SD). Endotoxin contamination was determined to be below 0.1 EU/mL by the Limulus assay test [22].

2.3. Technetium-99m (^{99m}Tc)-labeling of vesicles

Radiolabeling of vesicles was performed according to a method described previously [14,17,23,24]. A saline solution of sodium [^{99m}Tc]pertechnetate (5 mL, 2.78 GBq (75 mCi)) (GE Healthcare Radiopharmacy, San Antonio, TX) was injected into a vial containing lyophilized hexamethylpropyleneamine oxime (HMPAO; 0.5 mg, $SnCl_2$; 7.6 μg) (Ceretec™; GE Healthcare, Arlington, IL). The mixed solution was incubated for 5 min at room temperature. The ^{99m}Tc-HMPAO solution (1 mL) was then added to the vesicle dispersion ([lipids] = 7 g dL^{-1}, 1 mL), and the resulting mixture was incubated for 1 h. After removing free ^{99m}Tc-HMPAO by gel filtration (Sephadex-G25 column), total radioactivity was measured in a dose calibrator (Radex, Mark 5 Model, Houston, TX) and the labeling efficiency was calculated as the percentage of radioactivity in ^{99m}Tc-vesicles to radioactivity measured just before gel filtration.

Please cite this article as: Sou K, et al. Selective uptake of surface-modified phospholipid vesicles by bone marrow macrophages *in vivo*. Biomaterials (2007), doi:10.1016/j.biomaterials.2007.01.041

2.4. Labeling stability of ^{99m}Tc-labeled vesicles in vitro

Labeling stability was examined *in vitro* according to a previously reported procedure [25]. Prepared ^{99m}Tc-labeled vesicle dispersions (0.5 mL) were mixed with rabbit serum (1.5 mL) and incubated at 37 °C to check the labeling stability. A 100 μL aliquot of incubated sample at 24 and 48 h after mixing was passed through a Bio Gel A-15 m (200–400 mesh) spin column. The sample was eluted by sequential addition of 100 μL of Dulbecco's phosphate-buffered saline (pH 7.3) under the centrifugal force of 1000 rpm for 1 min. Each fraction was collected separately and counted in a scintillation well counter (Canberra multichannel analyzer; Canberra Industries, Meriden, CT). Another 100 μL aliquot of incubation sample was used as a standard. The sum total of activity eluted with vesicle fractions was compared with total radioactivity in the standard. As for ^{99m}Tc-labeled PEG(0.6)-[SA-Ve], the labeling stability was also examined in human plasma at 37 °C for 24 h.

2.5. Animal experiments

Animal experiments were performed under the National Institutes of Health Animal Use and Care guidelines and approved by the University of Texas Health Science Center at San Antonio Institutional Animal Care Committee. Male New Zealand White rabbits (2–3 kg, $n = 3$–4 per each vesicle formulation) were anesthetized with an intramuscular injection of ketamine/xylazine (both from Phoenix Scientific, St. Joseph, MO) mixture (50 and 10 mg/kg body weight (b.w.), respectively). One ear of a rabbit was catheterized with a venous line, and the other ear was catheterized with an arterial line. ^{99m}Tc-vesicles were infused into the venous line at 1 mL/min and blood samples were drawn from the arterial line. Each rabbit received a total dose of 214.6–377.4 MBq (5.8–10.2 mCi) ^{99m}Tc-activity and 15 mg/kg b.w. of lipids. As a control study, ^{99m}Tc-HMPAO solution (3 mL) was mixed with glutathione solution (30 mM, 3 mL), and the mixed solution was infused into the venous line at 1 mL/min in rabbits. Each rabbit received a total dose of 321.9–399.6 MBq (8.7–10.8 mCi) ^{99m}Tc-activity.

2.6. Imaging study

Rabbits were placed in the supine position under a Picker (Cleveland, OH) large-field-of-view gamma camera using a low-energy all-purpose collimator and interfaced with a Pinnacle imaging computer (Medasys, Ann Arbor, MI). One-minute dynamic 64 × 64 pixel scintigraphic images were acquired over a continuous period of 1.5 h after the injection of ^{99m}Tc-vesicles. Static images were also acquired at various times post-injection. The image analysis was performed using a nuclear medicine analysis workstation (Pinnacle computer; Medasys, Ann Arbor, MI). The regions of interest were drawn around images of the whole body, one femur, liver, and spleen. The radioactivity counts were decay-corrected at each time, and converted to a percentage of whole body counts. Corrections were made for the blood pool contribution of each organ using the percent injected dose (%ID) measured immediately after infusion.

2.7. Blood persistence and biodistribution

Blood was collected from the arterial line of the rabbit (100 μL) at various times post-injection. The radioactivity of blood samples was quantified in a scintillation well counter (Canberra Multichannel Analyzer, Meridan, CT) during the same counting session. The counts at each time were converted to the percentage of the counts in the sample collected immediately after injection. The animals were rapidly sacrificed at 6 or 24 h and the tissue samples were collected, weighed and counted for radioactivity in the same scintillation well counter for calculation of biodistribution. To calculate the %ID per organ, total blood volume, muscle and skin mass were estimated as 5.7%, 45%, and 10% of total body weight, respectively [26,27]. Bone mass was estimated to be 12 times that of one femur [28].

2.8. Microscopic study

Histological examination of fluorescence delivered into bone marrow tissues was performed using PEG(0.6)-[SA-Ve], double fluorescently labeled by encapsulating SOD conjugated by TR sulfonyl chloride (TR-SOD) in inner aqueous phase and embedding C_1-BODIPY C_{12} in bilayer membrane. Conjugation of TR-SOD to SOD was performed according to previously reported procedure [29], and purified TR-SOD was encapsulated in mixed lipids including 1 mol% of C_1-BODIPY C_{12} to obtain the double fluorescently-labeled PEG(0.6)-[SA-Ve] with size of 247 ± 22 nm in diameter. Labeled vesicles were i.v. injected into anesthetized Male New Zealand White rabbits (2.5 kg, lipids: 15 mg/kg b.w.). At 6 h after injection, femoral bone marrow tissues, liver and spleen were taken, fixed in 10% formalin solution, and then sliced into sections. The sections were fixed on the glass slides with agar at 4 °C and examined with a confocal scanning microscope (Olympus IX-70). Transmission electron microscopic (TEM) observation was performed to observe the bone marrow tissues at a higher magnification. PEG(0.6)-[SA-Ve] were i.v. injected into anesthetized Male New Zealand White rabbits (2.5 kg). The rabbits received 15 mg/kg b.w. of lipids. Control rabbits received no injection. Bone marrow was taken from the left femur of rabbits at 6 h after injection of vesicles, and fixed in 2.5% glutaraldehyde solution. The fixed bone marrow was then washed with 0.1 mol/L phosphate buffer, pH 7.4, and stained with 2% osmic acid solution at 4 °C for 2 h. The organs were first dehydrated stepwise with ethanol, and then polymerized using Quetol 812 at 60 °C for 28 h. The obtained samples were sliced into sections by using an Ultracut S microtome. The sliced samples were stained with 3% uranyl acetate solution for 20 min and then treated with Satoh's lead solution (lead acetate, lead nitrate, and lead citrate) in citrate for 5 min, washed, and dried. The sample was observed and a picture taken with a transmission electron microscope (TEM, H-7500, Hitachi, Tokyo, Japan).

2.9. Theoretical estimation

The theoretical estimation for surface coverage by PEG on vesicles has been reported previously [30,31]. At low grafting densities of PEG, the chains of grafted-PEG are displayed "mushrooms", in which area A_{PEG} covered by each molecule is theoretically calculated as

$$A_{PEG} = \pi R_F^2, \tag{1}$$

where the Flory radius R_F is given by

$$R_F = N^{3/5} a, \tag{2}$$

where N is the degree of polymerization, a is the size of a monomer.

The percentage of covered surface area by PEG in the mushroom conformation R was estimated as

$$R = A_{PEG} \times M / A_{lipid}, \tag{3}$$

where M is the mole percentage of PEG-DSPE and A_{lipid} is the average area of total membrane lipids. In subsequent calculation, we used $N = 114$ and $a = 0.35$ nm for PEG (Mw 5000), and $A_{lipid} \approx 0.4\,nm^2$ for average area as mixed membrane of DPPC and CH (1:1 molar ratio) [32].

2.10. Statistical methods

Values are reported as mean ± standard error of the mean (SEM). Statistical analysis was performed using Microsoft Excel for Windows. Biodistribution data were compared using the Student's unpaired t-test. A p-value <0.01 or 0.05 was considered statistically significant.

Please cite this article as: Sou K, et al. Selective uptake of surface-modified phospholipid vesicles by bone marrow macrophages *in vivo*. Biomaterials (2007), doi:10.1016/j.biomaterials.2007.01.041

3. Results

3.1. Surface modification and radiolabeling

The average diameter of vesicles was controlled to 270 nm by the stepwise extrusion through cellulose acetate membrane filters with a final pore size of 0.22 μm as shown in Table 1. The surface of the vesicles were modified during spontaneous incorporation of PEG conjugated to 1,2-distearoyl-*sn*-glycero-3-phosphoethanolamine (DSPE) into the lipid bilayer of preformed vesicles. The incorporation efficiency of PEG-DSPE was approximately 85%, independent of the added amount. Theoretically, the surface of PEG (0.3)-[SA-Ve] is not fully covered with PEG chains in mushroom conformation (theoretically calculated covered surface area: 85%), and surface coverage is completed with >0.6 mol% of PEG-DSPE. The ^{99m}Tc-labeling efficiency was approximately 84%, independent of the vesicular formulation. Since the ^{99m}Tc was located in the inner aqueous phase of vesicles encapsulating glutathione, the surface properties would not have been altered by the labeling procedure. The incubation of labeled ^{99m}Tc-vesicles in rabbit serum for 48 h revealed that more than 95% of the incorporated ^{99m}Tc remained in the prepared vesicles, regardless of the composition of the vesicles. Also in human plasma, 98% of incorporated ^{99m}Tc remained with PEG(0.6)-[SA-Ve] at 24 h. These data indicate that the labeling procedure results in a stably labeled vesicle preparation and maintains the ^{99m}Tc within vesicles, even during incubation in plasma at 37 °C.

3.2. Circulation kinetics and biodistribution

First, the circulation kinetics and organ distribution of several formulations were compared to determine the optimized component for targeting bone marrow. For this purpose, scintigraphy was superior to other methods because it was possible to quantitatively determine the organ distribution of the injected vesicles in whole body. The elimination rate of SA-Ve from circulating blood was much faster compared with that of control vesicles (Ve): the circulating half-life times ($t_{1/2}$s) of the SA-Ve and Ve were 0.6 and 9.4 h at injection dose of 15 mg/kg b.w. (Fig. 1(A)). Incorporation of as little as 0.3 mol% of PEG-DSPE did not affect the circulation time of SA-Ve. Incorporation of above 0.6 mol% of PEG-DSPE prolonged the circulation time of SA-Ve and the $t_{1/2}$ increased with increasing amounts of PEG-DSPE incorporation as summarized in Table 1. The incorporation of 2.6 mol% of PEG-DSPE also gave a remarkable improvement in circulation time for control Ve ($t_{1/2}$: 24.8 h). At 24 h post injection, the radioactivity of excised organs was counted using a scintillation counter. Major organs exhibiting the uptake of vesicles were bone marrow and liver for SA-Ve (Figs. 1(B) and (C)), while liver and spleen were the organs with the highest accumulation of control Ve (Figs. 1(C) and (D)). PEG modification clearly inhibited hepatic uptake of both SA-Ve and control Ve, and this effect became significant as the amount of PEG-DSPE incorporated increased (Fig. 1(C)). While a maximum amount of SA-Ve was observed in bone marrow when the SA-Ve contained 0.6 mol% PEG-DSPE, further incorporation of PEG-DSPE led to a decrease in the distribution of SA-Ve in bone marrow (Fig. 1(B)). Other organs apart from kidney and muscle for PEG(2.6)-[SA-Ve] exhibited only a small amount of activity (<1%ID, Supplementary Table 1 online). Injection in rabbits of a mixed solution of ^{99m}Tc-HMPAO and glutathione in a similar ratio as would be found within ^{99m}Tc-vesicles served as a control study of the radiolabeling agents without encapsulation within the vesicles. As shown in Fig. 2(A), injection of ^{99m}Tc-HMPAO/glutathione was rapidly eliminated from blood circulation ($t_{1/2}$: 3 min), and gamma camera images indicated that the labeling agents were rapidly excreted in urine through the kidney (Fig. 2(B)). Region of interest analysis showed that 67.1±0.8% of injected radioactivity was detected in bladder within 1 h after injection (Fig. 2(C)). At 6 h, biodistribution data also showed significant radioactivity in the urine (76.91±4.80%ID) and kidney (6.11±0.53%ID), but other organs including bone marrow had only minimal %ID dose uptake as summarized in Table 2. This control study shows that a mixture of ^{99m}Tc-HMPAO and glutathione is rapidly removed from the blood by renal excretion, which is

Table 1
Specification of prepared vesicles

Sample[a]	Mean diameter±SD (nm)	PEG-DSPE (mol%)	$t_{1/2}$ (h)[b]
SA-Ve	269±11	0	0.6
PEG(0.3)-[SA-Ve]	276±13	0.3	0.6
PEG(0.6)-[SA-Ve]	273±12	0.6	1.0
PEG(1.4)-[SA-Ve]	275±12	1.4	3.9
PEG(2.6)-[SA-Ve]	274±12	2.6	5.4
Ve	262±43	0	9.4
PEG(2.6)-Ve	259±74	2.6	24.8

[a]SA-Ve is based on DPPC/CH/SA (molar ratio, 1:1:0.2), and Ve is DPPC/CH (molar ratio, 1:1) as a control sample. PEG-modified samples were prepared using the spontaneous incorporation of PEG-DSPE into the prepared SA-Ve or Ve.
[b]The $t_{1/2}$ values were calculated from Fig. 1(A) data.

Please cite this article as: Sou K, et al. Selective uptake of surface-modified phospholipid vesicles by bone marrow macrophages *in vivo*. Biomaterials (2007), doi:10.1016/j.biomaterials.2007.01.041

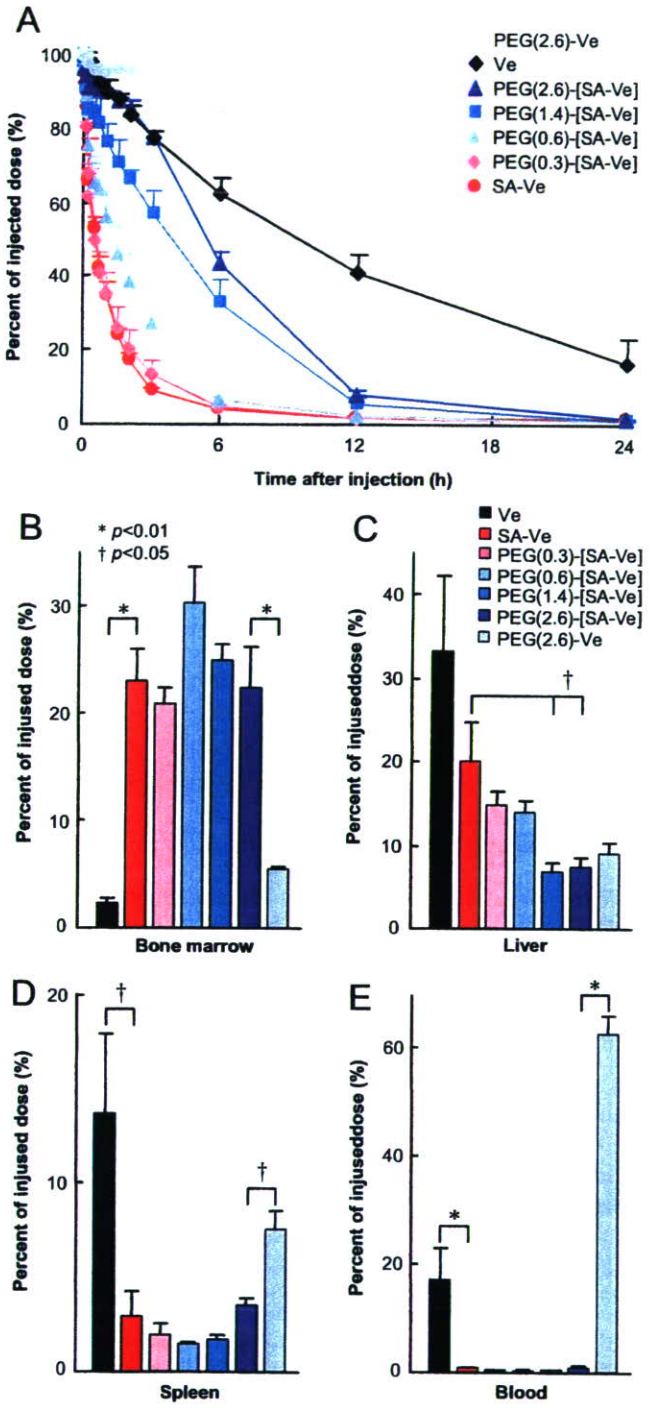

Fig. 1. Effect of surface modification with SA and PEG-DSPE on circulation kinetics and organ distribution of phospholipid vesicles. (A) Circulation kinetics of SA-vesicles (SA-Ve) and control vesicles (Ve) containing various amounts of PEG-DSPE after i.v. infusion (lipids: 15 mg/kg b.w.) in rabbits. ^{99m}Tc radioactivity was quantitated by scintillation counting of blood samples with time. The percentage of injected dose was calculated as a percentage of baseline radioactivity in a blood sample withdrawn just after injection. (B)–(E) Distribution of SA-vesicles (SA-Ve) and control vesicles (Ve) containing various amounts of PEG-DSPE as a percentage of the injected dose in bone marrow (B), liver (C), spleen (D), and blood (E) at 24 h after i.v. infusion in rabbits. *, Statistical significance ($p<0.01$), †, statistical significance ($p<0.05$).

typical of small molecules. These results indicate that the SA-Ve were clearly directed to bone marrow, and the process of accumulation of SA-Ve into bone marrow is correlated with competitive trapping by liver. Surface modification of SA-Ve with the proper amount of PEG-lipids inhibits the trapping of SA-Ve in liver and directs SA-Ve to bone marrow, a process which could be regarded as a combination of active and passive targeting. Conventional anionic vesicles containing phosphatidyl glycerol (PG) were inactive for targeting of bone marrow (Supplementary Table 2 online). The injected PEG(0.6)-[SA-Ve], which was the formulation showing the highest persistence in bone marrow at 24 h, were almost removed from circulation within 6 h (as little as 6.4±0.5%ID of PEG(0.6)-[SA-Ve] was circulating in blood at 6 h). Therefore, the initial distribution kinetics of PEG(0.6)-[SA-Ve] was studied in detail.

3.3. Distribution kinetics of PEG(0.6)-[SA-Ve]

Scintigraphic images clearly showed the injected radioactivity of PEG(0.6)-[SA-Ve] to be redirected from heart and liver, both organs having large blood pool contributions, and increasingly deposited in the bone marrow over time (Fig. 3(A)). The distribution kinetics in bone marrow, liver, and spleen, analyzed from the scintigraphic images, quantitatively indicated that significantly higher doses had accumulated in bone marrow, reaching 68.5±3.3%ID by 6 h after injection (Fig. 3(B)). The biodistribution data calculated from the radioactivity of excised organs also showed that 69.74±0.3%ID of PEG(0.6)-[SA-Ve] had accumulated in bone marrow, as shown in Table 2. At the same time point, liver and spleen had much smaller amounts of 11.51±2.88 and 5.00±1.19%ID, respectively. When ^{99m}Tc-HMPAO/glutathione was injected without encapsulation into PEG(0.6)-[SA-Ve], bone marrow, liver, and spleen had only 1.13±0.24, 1.52±0.14, and 0.01±0.00%ID, respectively. The isolated femur was further separated into soft bone marrow, joint bone (sponge bone), and skeleton and each separate tissue counted for radioactivity. As shown in Fig. 3(C), 66.5±1.1% of radioactivity in one femur was detected in soft bone marrow. The joint bone including soft bone marrow had 28.8±1.3% of radioactivity, and less radioactivity was detected in the separated skeleton (4.7±0.3%). These results indicate that the intravenously injected PEG(0.6)-[SA-Ve] mostly accumulates into soft bone marrow. The gamma camera images clearly show that the bone marrow uptake was evenly distributed over whole bone (Fig. 4), and the localization of radioactivity representing the distribution of PEG(0.6)-[SA-Ve] in these images was analyzed for separate regions. The spine and pelvis had 21.23±0.42% and 18.09±0.60%, values which were much higher than other regions. The right and left femurs had equal radioactivity of 7.97±0.05% and 8.34±0.18%; these values are in agreement with a report

Please cite this article as: Sou K, et al. Selective uptake of surface-modified phospholipid vesicles by bone marrow macrophages *in vivo*. Biomaterials (2007), doi:10.1016/j.biomaterials.2007.01.041

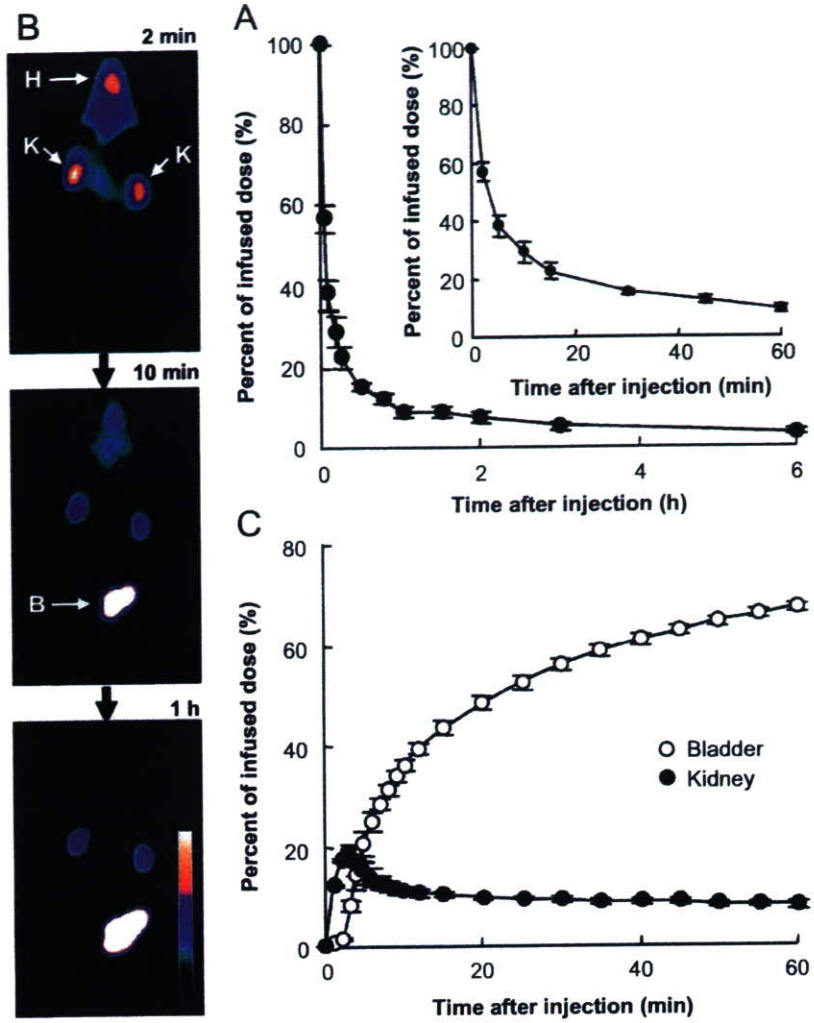

Fig. 2. Circulation and distribution kinetics of mixture of ^{99m}Tc-HMPAO and glutathione without encapsulation in vesicles after i.v. infusion in rabbits. (A) Circulation kinetics (B) Gamma camera images of rabbits acquired at various times after infusion. H: heart, K: kidney, B: bladder. (C) Distribution profiles as a percentage of the injected dose analyzed from the gamma camera images.

describing the relationship of 12 times that of a femur as being equivalent to whole bone in rabbits [28].

3.4. *Microscopic localization of PEG(0.6)-[SA-Ve] in bone marrow*

The initial studies were designed to demonstrate that PEG(0.6)-[SA-Ve] functions as a nanoparticulate carrier as well as identify their microscopic localization in tissues. We used PEG(0.6)-[SA-Ve] double-labeled by encapsulating water-soluble TR-SOD in an aqueous phase and embedding lipid-soluble C_1-BODIPY C_{12} in bilayer membrane (Fig. 5(A)). As shown in Fig. 5(B), the bone marrow sections have fluorescence from both the TR-SOD and C_1-BODIPY C_{12}. The fluorescence was locally concentrated, and larger fluorescent domain was 30 μm in size along the long axis. Fluorescent distribution in red pulp of spleen was dense, whereas it was sparse in liver. An important finding from this observation is that the fluorescence from membrane probes and encapsulated probes are co-localized in bone marrow. These images clearly indicate that PEG(0.6)-[SA-Ve] functions as a nanoparticle-carrier to deliver the encapsulated agents to bone marrow tissues. A second study was performed to identify the histological location of PEG(0.6)-[SA-Ve] in bone marrow. Femoral bone marrow tissue was taken from rabbit at 6 h after i.v. injection of PEG(0.6)-[SA-Ve] and examined using TEM. TEM observation clearly demonstrated the location of PEG(0.6)-[SA-Ve] in bone marrow (Figs. 6(A) and (B)). A massive number of vesicles were trapped in endosomes and lysosomes of BMMϕ, but no vesicles were observed in cytoplasm and cell nucleus (Fig. 6(B)). The diameter of these vesicles averaged 270 nm which was the original diameter of the intravenously administered PEG(0.6)-[SA-Ve]. Several similar BMMϕ with vesicles in endosomes and lysosomes were observed, while no vesicles were observed

Please cite this article as: Sou K, et al. Selective uptake of surface-modified phospholipid vesicles by bone marrow macrophages *in vivo*. Biomaterials (2007), doi:10.1016/j.biomaterials.2007.01.041

Table 2
Biodistribution of PEG(0.6)-[SA-Ve] and ^{99m}Tc-HMPAO/glutathione as a percent of the injected dose (%ID) and %ID per gram of tissue at 6 h after i.v. infusion in rabbits

Organs	PEG(0.6)-[SA-Ve]		^{99m}Tc-HMPAO/glutathione	
	%ID ± SEM (%)	%ID/g tissue ± SEM (%/g)	%ID ± SEM (%)	%ID/g tissue ± SEM (%/g)
Blood	6.58 ± 2.91	0.065 ± 0.028	3.34 ± 1.68	0.025 ± 0.013
Bone marrow	69.74 ± 0.86	0.806 ± 0.048	1.13 ± 0.24	0.010 ± 0.001
Liver	11.51 ± 2.88	0.237 ± 0.067	1.52 ± 0.14	0.022 ± 0.001
Spleen	5.00 ± 1.19	5.387 ± 0.807	0.01 ± 0.00	0.011 ± 0.001
Bowel	5.85 ± 0.31	0.014 ± 0.000	4.41 ± 0.19	0.009 ± 0.000
Skin	1.57 ± 0.21	0.009 ± 0.001	2.34 ± 0.30	0.010 ± 0.001
Kidney	2.40 ± 0.10	0.148 ± 0.011	6.11 ± 0.53	0.440 ± 0.066
Muscle	1.86 ± 0.17	0.003 ± 0.000	2.60 ± 0.63	0.002 ± 0.001
Lung	0.19 ± 0.03	0.024 ± 0.006	0.12 ± 0.03	0.010 ± 0.001
Heart	0.03 ± 0.01	0.010 ± 0.002	0.03 ± 0.01	0.006 ± 0.001
Brain	0.01 ± 0.00	0.002 ± 0.000	0.01 ± 0.00	0.001 ± 0.000
Testis	0.03 ± 0.01	0.024 ± 0.005	0.02 ± 0.00	0.008 ± 0.002
Urine	3.57 ± 1.74	—	76.91 ± 4.80	—

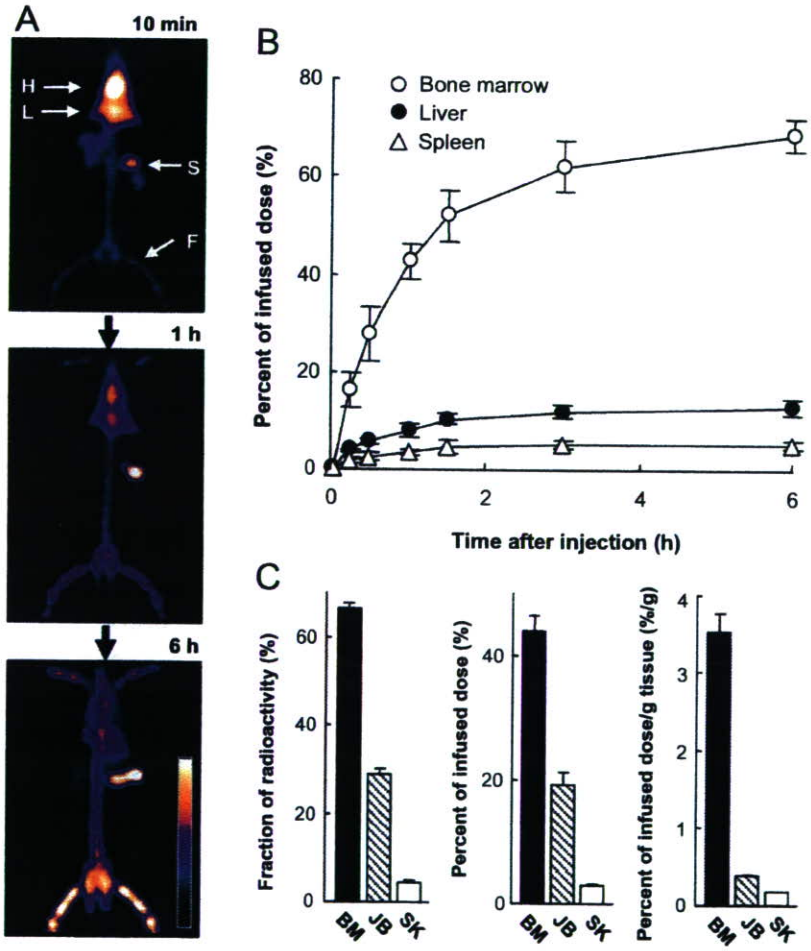

Fig. 3. Initial distribution kinetics of PEG(0.6)-[SA-Ve] after i.v. infusion (lipids: 15 mg/kg b.w.) in rabbits. (A) Gamma camera images of rabbits acquired at various times after infusion. H: heart, L: liver, S: spleen, F: femur. (B) Distribution profiles as a percentage of the injected dose analyzed from the gamma camera images. The total bone marrow was estimated to be 12 times that of one femur. (C) Distribution of radioactivity of PEG(0.6)-[SA-Ve] in separated soft bone marrow (BM), joint bone (sponge bone) (JB), and skeleton (SK) of one femur collected at 6 h after i.v. infusion. Three panels show the fraction of radioactivity, percent of injected dose (%ID), and %ID/g tissue, respectively.

Please cite this article as: Sou K, et al. Selective uptake of surface-modified phospholipid vesicles by bone marrow macrophages *in vivo*. Biomaterials (2007), doi:10.1016/j.biomaterials.2007.01.041

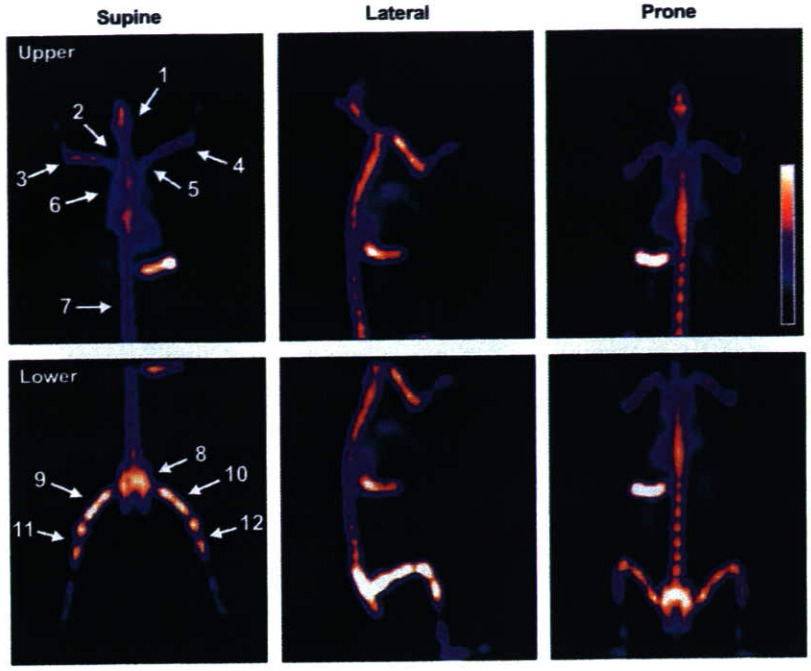

Fig. 4. Gamma camera images of rabbit receiving PEG(0.6)-[SA-Ve], acquired from various angles at 6 h after i.v. infusion. Bone marrow is clearly displayed in these images throughout the rabbit body. Relative radioactivity in separated bone parts were calculated to 1; head (8.41 ± 1.58%), 2; neck (1.10 ± 0.11%), 3; right arm (5.72 ± 0.33%), 4; left arm (5.54 ± 0.40%), 5; shoulder (3.62 ± 0.69%), 6; sternum (4.11 ± 1.35%), 7; spine (21.23 ± 0.42%), 8; pelvis (18.09 ± 0.60%), 9; right femur (7.97 ± 0.05%), 10; left femur (8.34 ± 0.18%), 11; distal right foot (7.88 ± 0.25%), and 12; distal left foot (7.98 ± 0.33%) as percentages to radioactivity of whole bone ± SEM.

in other types of cell such as granular leukocytes, erythroblasts, and endothelial cells in observed section. These microscopic localization studies demonstrate that BMMϕ are the cellular components responsible for clearance of vesicles from the circulation and their uptake by the bone marrow.

4. Discussion

These studies demonstrate that PEG-[SA-Ve] are efficient carriers for targeting the BMMϕ. These vesicles should be useful in the development of bone marrow targeted agents for therapeutic applications. Additionally, this *in vivo* model appears to be an ideal model with which to investigate the role of BMMϕ in the hematopoietic environment. The radiolabeling method for the vesicles encapsulating glutathione with ^{99m}Tc-HMPAO has previously been established for imaging studies [14,23,24]. In the present vesicle formulation, we confirmed the stability of the ^{99m}Tc radiolabeled-vesicles during incubation in serum and plasma at 37 °C for 48 h (more than 95% remaining with vesicles), and we also determined that the free labeling agent is not specifically distributed into organs such as bone marrow, liver, and spleen, but rapidly eliminated through renal excretion as shown in Fig. 2 and Table 2. This evidence provides strong support that the radioisotope distribution reflects the true biodistribution of vesicles. As shown in Fig. 1, comparative data showing the organ distribution of several formulations clearly demonstrated that the uptake of vesicles by bone marrow is induced by the incorporation of SA ($p < 0.01$); furthermore, the incorporation of a small amount of PEG-DSPE on the surface of SA-Ve prolongs its circulation time and tends to enhance the bone marrow selectivity by preventing hepatic uptake. Thus, maximum distribution to bone marrow was observed at 0.6 mol% PEG-DSPE (Fig. 1(B)). The degree of hepatic uptake was reduced as the PEG-DSPE content increased, and this effect became significant above 1.4 mol% ($p < 0.05$). Bone marrow uptake was also reduced above 1.4 mol%. In general, 5–10 mol% of PEG-lipids is incorporated into most of the long circulating vesicle formulations for passive targeting [8,9]. In the present study, prolonged circulation time of vesicles was observed above 0.6 mol% of PEG-DSPE, and the circulation times were prolonged more in vesicles with higher PEG-DSPE content. For the effective targeting of bone marrow, however, higher concentrations of PEG blocked the active targeting of the vesicles to bone marrow. These results indicate that the dense PEG layer on the vesicular surface covers the surface properties having the character of SA and depress uptake by BMMϕ. Therefore, the optimal amount of PEG incorporation was found to be 0.6 mol%, as this concentration passively enhances active targeting. Theoretically, approximately 0.4 mol% of PEG (Mw 5000)-lipids is estimated to be the critical content required to fully cover the vesicle surface which consists of DPPC and CH (1:1 molar ratio) with the mushroom conformation of PEG chains from Eqs. (1) to (3). Thus, it is

Please cite this article as: Sou K, et al. Selective uptake of surface-modified phospholipid vesicles by bone marrow macrophages *in vivo*. Biomaterials (2007), doi:10.1016/j.biomaterials.2007.01.041

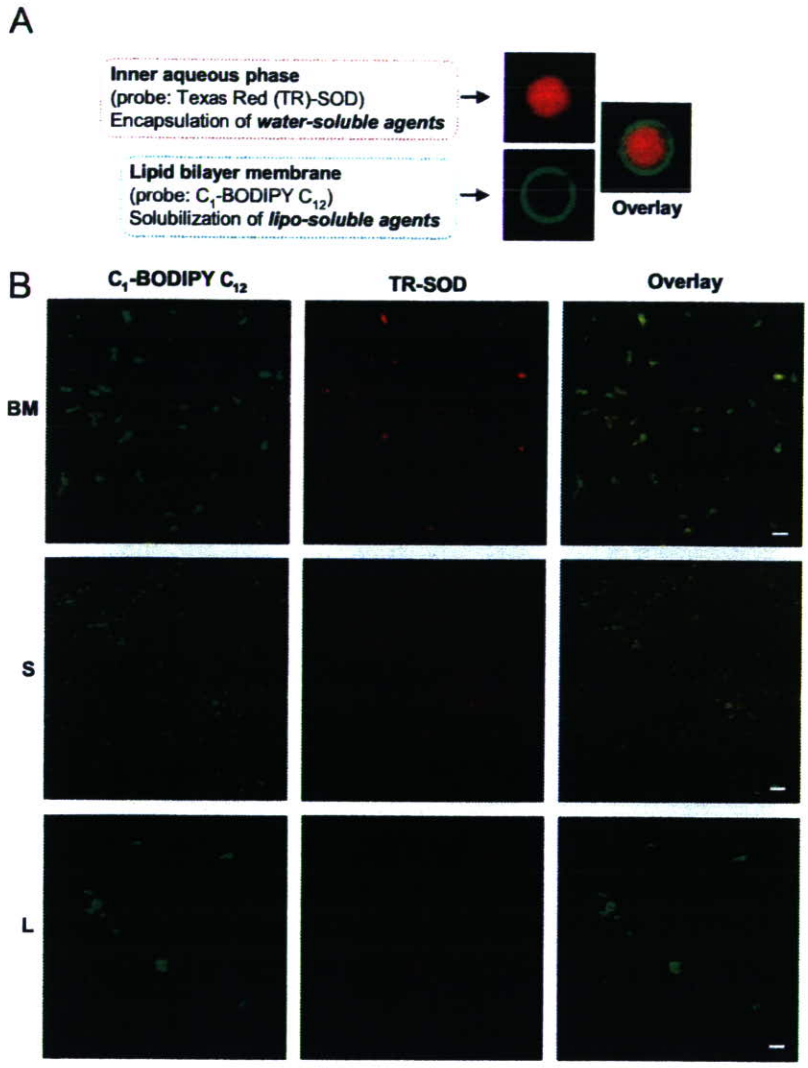

Fig. 5. Histological examination of fluorescence delivered into bone marrow tissues using PEG(0.6)-[SA-Ve] as carriers. (A) Fluorescence localization in double fluorescence-labeled large multilamellar PEG(0.6)-[SA-Ve] with diameter of ca. 10 μm. This observation was performed before extrusion to submicron size to enable observation of the structure within resolution of a confocal microscope. This image indicates that red fluorescence comes from TR-SOD which is encapsulated in inner aqueous phase and green fluorescence comes from C_1-BODIPY C_{12} which is embedded in bilayer membrane. (B) Confocal scanning images of femoral bone marrow (BM), spleen (S), and liver (L) taken from rabbit at 6 h after i.v. injection of double fluorescence-labeled PEG(0.6)-[SA-Ve] with size of 247±22 nm in diameter (lipids: 15 mg/kg b.w.). The scale bars represent 20 μm.

estimated that the optimal incorporation amount of PEG-lipids is slightly higher than that required to fully cover the vesicular surface. This finding provides useful information for the design of vesicle surface to passively enhance the active targeting with PEG-modification *in vivo*.

To examine the participation of the anionic properties of vesicles in BMMϕ uptake, we investigated the organ distribution of conventional anionic vesicles containing PG with same protocol. These PG-vesicles do not distribute to the bone marrow (Supplementary Table 2 online, only 5.36±0.65%ID of PG-vesicles were taken up by the bone marrow at 24 h after i.v. injection). Comparative data for Ve and SA-Ve are shown in Fig. 1(B) and Supplementary Table 1. Previous publications have also supported the observation that PG-vesicles do not distribute to the bone marrow [33], and neutral vesicles with various sizes in the range of 136.2–318 nm do not distribute to the bone marrow [34]. These results indicated that the targeting of bone marrow is not general for neutral vesicles and is achieved not only by the anionic surface of vesicles. The results suggest that SA is specifically responsible for the bone marrow targeting.

Histological observations showed that the vesicles and encapsulated agents are distributed at the same locations into bone marrow tissues, clearly indicating that the encapsulated agents were delivered to the bone marrow tissues by the vesicles (Fig. 5). Higher magnification TEM observations have demonstrated that a massive number of vesicles are trapped in the endosomes and lysosomes of the BMMϕ (Fig. 6). These observations indicated that the

Please cite this article as: Sou K, et al. Selective uptake of surface-modified phospholipid vesicles by bone marrow macrophages *in vivo*. Biomaterials (2007), doi:10.1016/j.biomaterials.2007.01.041

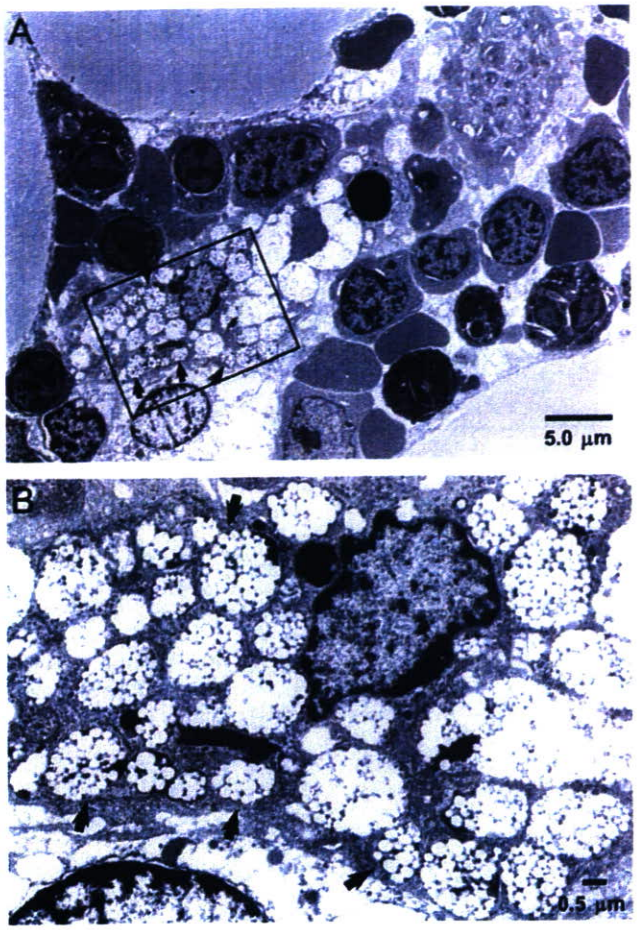

Fig. 6. Transmission electron micrographs of femoral bone marrow tissue section, taken from rabbit at 6 h after i.v. injection of PEG(0.6)-[SA-Ve] (lipids: 15 mg/kg b.w.). (A) Low magnified micrograph representing the bone marrow tissue including macrophage and various bone marrow cells. (B) High magnified micrograph of framed region in panel (A). A massive number of vesicles with original diameter (average 270 nm) are trapped in several endosomes or lysosomes of macrophage. Some are indicated by arrows, which shows same position in (A) and (B).

uptake of PEG(0.6)-[SA-Ve] by bone marrow was responded by the endocytosis of BMMϕ. One potent trigger to accelerate the cellular endocytosis for vesicles is an interaction with the receptors on the surface of cells, that are known as a receptor-mediated endocytosis which is investigated as a potent pathway for drug targeting to specific cell including macrophage [2,10,11]. Scavenger receptors are membrane glycoproteins that are present mainly on cells of the macrophage lineage [35,36]. Various polyanionic compounds such as dextran sulfate, polyinosinic acid, and acetylated low density lipoproteins have been reported as ligands for this receptor [37,38]. These compounds are taken at high levels by macrophages via a scavenger receptor-mediated mechanism. On the other hand, many polyanions such as chondroitin sulfate, poly(D-glutamic) acid, and polycytidylic acid are not ligands for scavenger receptors [37,38]. Previous investigations indicated that the scavenger receptors on macrophages contribute to the recognition of polyanionic structures, resulting in selective uptake. Enhanced uptake of succinylated proteins has been investigated in cultured brain microvessel endothelial cells. Endothelial cells also express the scavenger receptor on their surface. Large succinylated proteins such as catalase (Mw 227 kDa) and bovine serum albumin (Mw 70 kDa) were taken up by the cells via a scavenger receptor-mediated mechanism, whereas significant uptake was not observed for native proteins and small succinylated proteins such as SOD (Mw 34 kDa) and soybean trypsin inhibitor (Mw 21 kDa) [39]. This indicates that succinylation of large molecules is involved in the uptake via a scavenger receptor-mediated mechanism. Recently, Szabó et al. reported the uptake of branched polypeptides by bone marrow culture-derived murine macrophages. They indicated that the succinylation of branched polypeptides significantly enhanced the uptake by macrophages, and the uptake was inhibited by blocking of the class-A scavenger receptors [40]. Because the terminal hydrophilic head group of SA is corresponding to the succinylated structure, we speculate that the interaction between PEG-[SA-Ve] and the scavenger receptors on BMMϕ might participate in the selective uptake. However, further mechanistic investigation on uptake of PEG-[SA-Ve] by BMMϕ, splenic macrophages, and hepatic Kupffer cells is necessary to clarify the mechanism of organ selective macrophage uptake.

Previous pharmacokinetic studies have been performed using vesicles containing SA that have the same lipid composition as in the present study with PEG(0.3)-[SA-Ve], but a significantly higher dose was employed (lipids: 680 mg/kg b.w.) [17]. In these studies, the bone marrow-selective distribution was not observed, so it appears that the bone marrow selectivity is limited by the injection dosage in certain applications. As the vesicle dosage increases, the MPS in the bone marrow becomes saturated; as a result, liver and spleen uptake is increased. In our previous organ distribution study in rabbits, >50%ID of the vesicles were still in circulation at 48 h after infusion of a massive dose of vesicles, while the bone marrow had 7.36 ± 0.34% of 680 mg/kg b.w. at the same time point [17]. This value is equivalent to 50.0 mg/kg b.w., and it can be used to estimate the maximum uptake capacity of MPS for vesicles. When vesicle dosage increases above 50.0 mg/kg b.w., the bone marrow is the first organ to become saturated, and the accumulation of vesicles then increases in the liver and spleen. Such sequential saturation of the MPS eliminates organ selectivity. Therefore, the bone marrow targeting of SA-Ve becomes striking when the dose of vesicles is below the saturation dosage for bone marrow, as observed in the present study (15 mg/kg b.w.). The ability of vesicular nanoparticles to encapsulate a wide variety of agents provides significant opportunities for bone marrow delivery applications. In the present study, we have demonstrated the delivery of scintigraphic and fluorescence imaging agents to bone marrow by using the

Please cite this article as: Sou K, et al. Selective uptake of surface-modified phospholipid vesicles by bone marrow macrophages *in vivo*. Biomaterials (2007), doi:10.1016/j.biomaterials.2007.01.041

SA-Ve vesicles. This method has advantages in delivering the therapeutic agents to treat bone marrow disorders.

5. Conclusion

This is the first report to show the organ distribution of PEG-[SA-Ve] at small dose injection. Organ distributions of several vesicular formulations were quantitatively compared to determine the component to induce the significant distribution into bone marrow. Our data have indicated that surface modification of phospholipid vesicles with two compounds, SA and PEG-DSPE, cooperatively induces the significant bone marrow targeting properties to vesicles. In this system, BMMϕ participated in the uptake of PEG-[SA-Ve], and the efficient delivery of the vesicles as encapsulating agents into the bone marrow was achieved within 6 h after injection. These results indicated that the PEG-[SA-Ve] is a potent carrier for drug delivery into BMMϕ *in vivo* and may be useful for delivering a wide range of therapeutic agents to bone marrow.

Acknowledgments

This work was partly supported by project of a Health and Labor Sciences Research Grant (Research on Pharmaceutical and Medical Safety, Artificial Blood Project) of the Ministry of Health, Labor and Welfare, Japan, and the Ministry of Education, Culture, Sports, Science and Technology, Grant-in-Aid for Scientific Research (B), 17300162, 2005. The authors gratefully acknowledge Dr. H. Sakai (Waseda University) for discussions on this research, Dr. Linda M. McManus (UTHSCSA) for assistance with electron microscopic images and Mr. R. Klipper (UTHSCSA) for technical support.

Appendix A. Supplementary materials

The online version of this article contains additional supplementary data. Please visit doi:10.1016/j.biomaterials.2007.01.041.

References

[1] Farokhzad OD, Jon S, Khademhosseini A, Tran TN, Lavan DA, Langer R. Nanoparticle–aptamer bioconjugates: a new approach for targeting prostate cancer cells. Cancer Res 2004;64:7668–72.

[2] Torchilin VP. Recent advances with liposomes as pharmaceutical carriers. Nat Rev Drug Discov 2005;4:145–60.

[3] Gregoriadis G, Wills EJ, Swain CP, Tavill AS. Drug-carrier potential of liposomes in cancer chemotherapy. Lancet 1974;1:1313–6.

[4] Felgner PL, Gadek TR, Holm M, Roman R, Chan HW, Wenz M, et al. Lipofection: a highly efficient, lipid-mediated DNA-transfection procedure. Proc Natl Acad Sci USA 1987;84:7413–7.

[5] Moghimi SM, Hunter AC, Murray JC. Long-circulating and target-specificity nanoparticles: theory to practice. Pharmacol Rev 2001;53:283–318.

[6] Sakai H, Horinouchi H, Tomiyama K, Ikeda E, Takeoka S, Kobayashi K, et al. Hemoglobin-vesicles as oxygen carriers: influence on phagocytic activity and histopathological changes in reticuloendothelial system. Am J Pathol 2001;159:1079–88.

[7] Fadok VA, Bratton DL, Rose DM, Pearson A, Ezekewitz RA, Henson PM. A receptor for phosphatidylserine-specific clearance of apoptotic cells. Nature 2000;405:85–90.

[8] Klibanov AL, Maruyama K, Torchilin VP, Huang L. Amphipathic polyethyleneglycols effectively prolong the circulation time of liposomes. FEBS Lett 1990;268:235–7.

[9] Gabizon A, Shmeeda H, Barenholz B. Pharmacokinetics of pegylated liposomal Doxorubicin: review of animal and human studies. Clin Pharmacokinet 2003;42:419–36.

[10] Turk MJ, Water DJ, Low PS. Folate-conjugated liposomes preferentially target macrophages associated with ovarian carcinoma macrophage. Cancer Lett 2004;213:165–72.

[11] Chellat F, Merhi Y, Moreau A, Yahia L'H. Therapeutic potential of nanoparticulate systems for macrophage targeting. Biomaterials 2005;26:7260–75.

[12] Mantovani A, Sozzani S, Locati M, Allavena P, Sica A. Macrophage polarization: tumor-associated macrophages as a paradigm for polarized M2 mononuclear phagocytes. Trends Immunol 2002;23:549–55.

[13] Allen TM, Austin GA, Chonn A, Lin L, Lee KC. Uptake of liposomes by cultured mouse bone marrow macrophages: influence of liposome composition and size. Biochim Biophys Acta 1991; 1061:56–64.

[14] Phillips WT, Klipper RW, Awasthi VD, Rudolph AS, Cliff R, Kwasiborski V, et al. Polyethylene glycol-modified liposome-encapsulated hemoglobin: a long circulating red cell substitute. J Pharmacol Exp Ther 1999;288:665–70.

[15] Dams ET, Oyen WJ, Boerman OC, Storm G, Laverman P, Kok PJ, et al. ^{99m}Tc-PEG liposomes for the scintigraphic detection of infection and inflammation: clinical evaluation. J Nucl Med 2000;41:622–30.

[16] Giuliani AL, Wiener E, Lee MJ, Brown IN, Berti G, Wickramasinghe SN. Changes in murine bone marrow macrophages and erythroid burst-forming cells following the intravenous injection of liposome-encapsulated dichloromethylene diphosphonate (Cl_2MDP). Eur J Haematol 2001;66:221–9.

[17] Sou K, Klipper R, Goins B, Tsuchida E, Phillips WT. Circulation kinetics and organ distribution of Hb-vesicles developed as a red blood cell substitute. J Pharmacol Exp Ther 2005; 312:702–9.

[18] Sadahira Y, Mori M. Role of the macrophage in erythropoiesis. Pathol Int 1999;49:841–8.

[19] Yoshida H, Kawane K, Koike M, Mori Y, Uchiyama Y, Nagata S. Phosphatidylserine-dependent engulfment by macrophages of nuclei from erythroid precursor cells. Nature 2005;437:754–8.

[20] Sou K, Naito Y, Endo T, Takeoka S, Tsuchida E. Effective encapsulation of proteins into size-controlled phospholipid vesicles using freeze–thawing and extrusion. Biotechnol Prog 2003;19:1547–52.

[21] Sou K, Endo T, Takeoka S, Tsuchida E. Poly(ethylene glycol)-modification of the phospholipid vesicles by using the spontaneous incorporation of poly(ethylene glycol)-lipid into the vesicles. Bioconjug Chem 2000;11:372–9.

[22] Sakai H, Hisamoto S, Fukutomi I, Sou K, Takeoka S, Tsuchida E. Detection of lipopolysaccharide in hemoglobin-vesicles by Limulus amebocyte lysate test with kinetic-turbidimetric gel clotting analysis and pretreatment of surfactant. J Pharm Sci 2004;93: 310–21.

[23] Rudolph AS, Klipper R, Goins B, Phillips WT. *In vivo* biodistribution of a radiolabeled blood substitute: ^{99m}Tc-labeled liposome-encapsulated hemoglobin in an anesthetized rabbit. Proc Natl Acad Sci USA 1991;88:10976–80.

[24] Phillips WT, Rudolph AS, Goins B, Timmons JH, Klipper R, Blumhardt R. A simple method for producing a technetium-99m-labeled liposome which is stable *in vivo*. Nucl Med Biol 1992;19:539–47.

Please cite this article as: Sou K, et al. Selective uptake of surface-modified phospholipid vesicles by bone marrow macrophages *in vivo*. Biomaterials (2007), doi:10.1016/j.biomaterials.2007.01.041